Geomorphology xxx (2016) xxx–xxx

Contents lists available at ScienceDirect

Geomorphology

journal homepage: www.elsevier.com/locate/geomorph

Subaqueous rock-avalanche deposits exposed by post-glacial isostatic rebound, Innfjorddalen, Western Norway

Markus Schleier [a,*], Reginald L. Hermanns [b,c], John C. Gosse [d], Thierry Oppikofer [b], Joachim Rohn [a], Jan F. Tønnesen [b]

[a] University of Erlangen-Nuremberg (FAU), GeoZentrum Nordbayern, Erlangen, Germany
[b] Geological Survey of Norway (NGU), Trondheim, Norway
[c] Norwegian University of Science and Technology, Department of Geology and Mineral Resources Engineering, Trondheim, Norway
[d] Dalhousie University, Department of Earth Sciences, Halifax, Canada

ARTICLE INFO

Article history:
Received 19 May 2015
Received in revised form 24 July 2016
Accepted 15 August 2016
Available online xxxx

Keywords:
Rock avalanches
Cosmogenic-nuclide dating
Dynamic runout modeling
Toma hills
Post-glacial isostatic rebound
Innfjorddalen
Norway

ABSTRACT

This paper presents a detailed description of deposits and landforms of multiple rock avalanches in Western Norway, one of which fell onto water-saturated sediments in Innfjorddalen below the former water level. Deposits of the latter are now exposed on the valley floor due to post-glacial isostatic rebound. At least three rock avalanches from the same source at Gråfonnfjellet Mountain have occurred during late glacial and post-glacial time, and their deposits are distributed over an area of 1.44 km^2 in the valley. These rock avalanches have volumes of 15.1×10^6 m^3, 5.4×10^6 m^3 and 0.3×10^6 m^3 and yielded cosmogenic radionuclide ^{10}Be ages of 14.3 ± 1.4 ka, 8.79 ± 0.94 ka and 1.028 ± 0.380 ka, respectively. The youngest event dates, within uncertainty limits to a historic rock avalanche in the year 1611–12 CE. The rock avalanches formed a stratified succession of deposits. The rock-avalanche deposits (1.38 m^2) have lobate forms, have frontal rims and parallel ridges, extend across the valley floor and up the opposite slope, and form dams on the valley floor. Isolated hills comprised of rock boulders (0.61 km^2), interpreted to be 'toma hills', are disconnected from the main rock-avalanche deposits by a 520-m-wide zone of deformed, valley-fill sediments. Trenches and a ground penetrating radar survey of these deposits indicate large-scale deformation or liquefaction. Numerical runout modeling of the rock avalanches with the code DAN3D supports the interpretation of their landforms and sources, and highlights their runout behavior.

1. Introduction

Large rock avalanches and their deposits have significantly impacted Quaternary landscape evolution in mountain areas (Hewitt et al., 2008, 2011), for example through the formation of rock-avalanche dams (Hewitt, 1998; Evans et al., 2011; Hermanns et al., 2011) and interactions with glacial processes (Hewitt, 2009a; Shulmeister et al., 2009; Shugar et al., 2012; Sosio et al., 2012; De Blasio, 2014; Delaney and Evans, 2014; Schleier et al., 2015) and related phenomena. Rock avalanches form continuous sheets of blocky debris and more unusual deposits and features that result from complex runout behavior and might not be easy to interpret. The processes affecting the mobility of granular flows including their complex emplacement histories and their interaction with erodible and deformable substrates along the path have been investigated widely by studying evidence of deformation in the field (Hewitt et al., 2008; Dufresne et al., 2010a; Hermanns et al., 2014), using analog experiments (Dufresne et al., 2010b, Dufresne, 2012) and numerical modeling (Crosta et al., 2009a, 2009b). Numerical dynamic runout modeling, for instance DAN3D, can be used to back-analyze rock avalanches and to study their runout behavior over complex three-dimensional terrain, and to predict future rock-avalanche runout (Hungr and Evans, 1996; McDougall and Hungr, 2004; Hungr, 2006; Sosio et al., 2008; Pedrazzini et al., 2012). Numerical modeling can also be used to support interpretations of the dynamics of prehistoric rock avalanches and associated landforms (Schleier et al., 2015).

Large rock-slope failures are common in the glacial overprinted mountain areas of Western Norway and are a hazard to people and infrastructure (Blikra et al., 2002, 2006; Braathen et al., 2004; Longva et al., 2009; Böhme et al., 2011; Hermanns et al., 2012a; Saintot et al., 2012; Oppikofer et al., 2013). Rock avalanches, in particular, are a threat due to their large energy release, long runout distances and possible secondary effects (Heim, 1932; Crosta et al., 2004; Evans et al., 2006, 2011; Hermanns and Longva, 2012).

Deposits of multiple rock avalanches are particularly common in the lower part of Innfjorddalen Valley (Schleier et al., 2013), and there is an

* Corresponding author at: GeoZentrum Nordbayern, Schlossgarten 5, 91054 Erlangen, Germany.
E-mail address: markus.schleier@fau.de (M. Schleier).

http://dx.doi.org/10.1016/j.geomorph.2016.08.024
0169-555X/

active unstable rock slope in the headwater area (Schleier et al., 2016; Fig. 1). Generally, as proposed by Hermanns et al. (2006), rock-slope failures could increase the probability of future failures in the vicinity because of accelerated decompression along the rock slope. Therefore, detailed integrative investigations of rock-avalanche deposits and landforms are useful for hazard assessments (Welkner et al., 2010), because they provide information on the temporal patterns of rock avalanches that can be compared to climate records (Hermanns et al., 2000; Trauth et al., 2000; Soldati et al., 2004; Blais-Stevens et al., 2011) and could be important for understanding post-failure behavior (Strom, 2006).

Typical rock-avalanche deposits have a carapace of angular rock boulders up to several meters across (Hewitt, 2009b). They include features indicative of high mobility such as frontal rims, lateral levees, parallel ridges, and run-up on the opposing valley sides (Evans et al., 1989; Erismann and Abele, 2001; Poschinger, 2002; Dufresne and Davies, 2009). Isolated hills of rock-avalanche material, termed 'tomas', have also been observed in front of some rock-avalanche sites (Abele, 1974; Poschinger, 2002; Poschinger et al., 2006; Dufresne et al., 2010a, 2010b; Masera et al., 2014).

A special case is rock avalanches that enter lakes or the sea. Their deposits are difficult to study because they lie below the water plane and thus cannot easily be accessed. In the case of Innfjorddalen, however, rock-avalanche deposits that entered a fjord have been raised above sea level due to post-glacial isostatic rebound of the Fennoscandian landmass (Fjeldskaar et al., 2000; Olsen et al., 2013).

This contribution builds on previous work on the Innfjorddalen rock avalanches by Seljesæter (2010) and Schleier et al. (2013), by presenting a detailed description of landforms in Innfjorddalen, new ^{10}Be cosmogenic ages and results of numerical runout modeling with DAN3D.

2. Regional setting

Innfjorddalen Valley is located in Møre og Romsdal County in Western Norway. It is an extension of the Innfjord, the head of which is located about 3.5 km NNE of the study area (Fig. 1). The valley has a typical glacial U-shaped cross-profile with oversteepened slopes and >1000 m of topographic relief (Fig. 2). The valley bottom lies at about 15 m a.s.l. and the highest peak (Gråfonnfjellet Mountain) has an elevation of 1475 m a.s.l.

The area is within the Western Gneiss Region of Norway, which is characterized by high-grade metamorphic rocks of the Caledonian Orogeny. Primary source rocks have been Proterozoic gneisses which have been partly covered by oceanic and continental sedimentary rocks (Hacker et al., 2010). The bedrock in Innfjorddalen comprises the typical hard gneisses of the region (Fig. 2) (Tveten et al., 1998): 1) quartz dioritic and partly migmatitic undifferentiated gneiss, 2) coarse-grained granitic gneiss, augen gneiss and gneissic granite, and 3) quartzitic gneiss, containing sillimanite and kyanite. The rocks have a well-developed metamorphic foliation that constitute surfaces along which rock slopes often have failed, for instance, main sliding surfaces (Henderson and Saintot, 2011; Saintot et al., 2011).

During the Pleistocene Epoch, the landscape of Western Norway was profoundly modified by glaciers. Typical landforms include U-shaped valleys, fjords, and cirques (Sollid and Sørbel, 1979; Fredin et al., 2013; Olsen et al., 2013). Besides erosive and sedimentary effects, these glaciations also had an impact on neotectonics, for instance, by crustal unloading and the following uplift (Olesen et al., 2013). The present-day distribution of marine sediments up to elevations of 220 m a.s.l. indicates that the Fennoscandian landmass has been glacio-isostatically raised several hundred meters since the Last Glacial Maximum (Fjeldskaar et al., 2000; Hansen et al., 2012, 2014; NGU, 2015). In Innfjorddalen Valley, the Late Pleistocene marine limit is about 120 m a.s.l. (Fig. 2). Uplift in the study area is continuing at rates of 2–3 mm/yr (Dehls et al., 2000) (Fig. 1) that can be a cause for crustal instability and seismicity and hence can trigger rock-slope failures (Blikra et al., 2002).

3. Materials and methods

3.1. Field mapping, granulometric description

Field mapping and landform interpretation in Innfjorddalen Valley were carried out, building on a Master's Thesis by Seljesæter (2010). The spatial distribution of rock-boulder deposits was mapped and the size, roundness, and sphericity of about 100 boulders in contact with one another were sampled at 13 locations. Boulder roundness and sphericity were described qualitatively using the classification of Pettijohn and Doornkamp (1973). Three trenches have been opened in the lower part of the valley to study the sedimentology and deformation of valley-fill sediments beside or below rock-avalanche deposits. The trenches were about 1.5 m wide, 1 m deep and up to 5 m long.

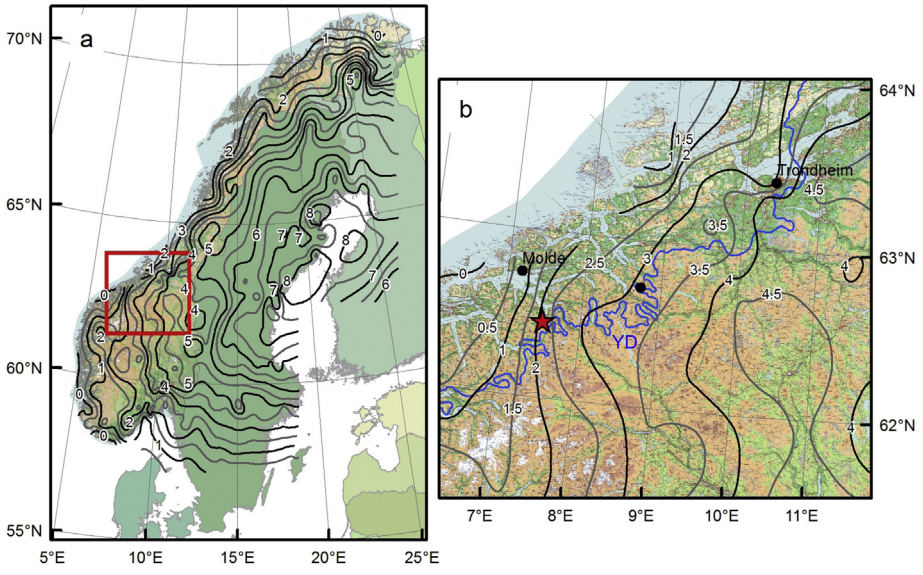

Fig. 1. Overview maps of Norway. (a) current apparent uplift rates in mm/yr (after Dehls et al., 2000). (b) Area of square in (a) showing location of Innfjorddalen (star), Younger Dryas ice extent (YD, after Sollid and Sørbel, 1979) and current apparent uplift rates in mm/yr.

Please cite this article as: Schleier, M., et al., Subaqueous rock-avalanche deposits exposed by post-glacial isostatic rebound, Innfjorddalen, Western Norway, Geomorphology (2016), http://dx.doi.org/10.1016/j.geomorph.2016.08.024

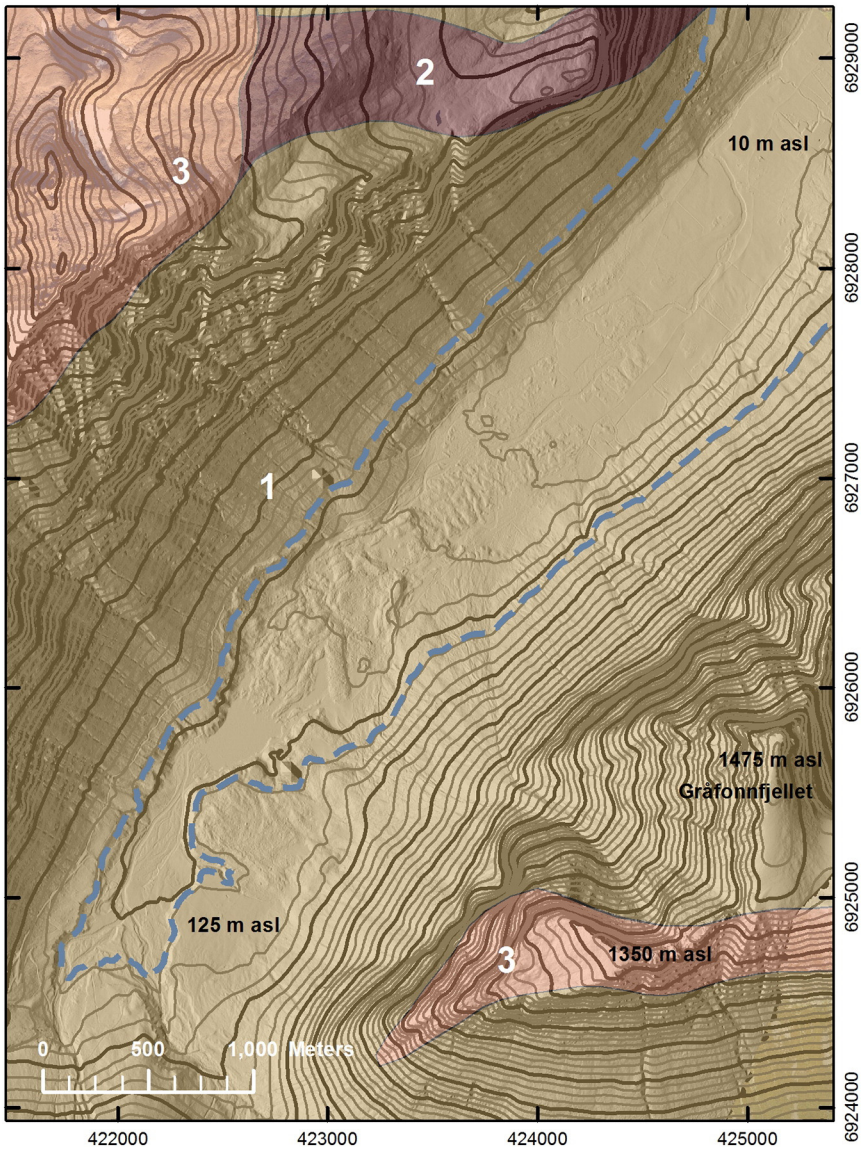

Fig. 2. Hillshade topographic map of Innfjorddalen (contour interval = 25 m) showing geologic units after Tveten et al. (1998): (1) undifferentiated quartz dioritic gneiss, partly migmatitic; (2) coarse-grained granitic gneiss, augen gneiss; (3) quartz-rich gneiss containing sillimanite and kyanite. The dashed line marks the approximate marine limit after NGU, 2015. (Coordinate system: WGS1984, UTM Zone 32N.)

3.2. Georadar profiling

A ground penetrating radar (GPR) survey was carried out by the Geological Survey of Norway to identify structures associated with the rock avalanches and to obtain subsurface information on successive rock-avalanche events (Mauring et al., 1998). Two transects totaling 1588 m in length were run on October 14, 2009. They include a 995-m-long valley-parallel transect along the main road and a 593-m-long transect across the valley along a track in the distal part of the rock-boulder deposits (see Fig. 5c for locations). The survey was performed with a pulseEkko 100 (instrument manufactured by Sensors & Software Inc.). The two antennae used in the survey, separated by 1 m, have a center frequency of 100 MHz and a transmitter output voltage of 1000 V. A measurement was made every 0.25 m along the profiles and a stacking of 4 was used at every measuring point. The time window of the measurements was 1200 ns. A CMP profile gave an average ground velocity of about 0.09 m/ns, which was used to calculate depths. A subjective gain has been applied manually to the GPR-data to achieve best results of the printing. Results are summarized in an unpublished database of the Geological Survey of Norway (NGU, 2009).

3.3. GIS surface analysis and topographic modeling

Orthophotos and digital elevation models (DEMs) were used to support and improve mapping and landform interpretation. The high-resolution orthophotos have a grid size of 0.5 m × 0.5 m, and the DEM, which was derived from airborne laser scanning, has a grid size of 2 m × 2 m. DEM derivatives such as slope angle, slope aspect, slope curvature, and hillshades (shaded relief maps) with different azimuths and altitudes for lighting were created to visualize the topography. The DEM was used as basis for topographic modeling to prepare input data for dynamic runout analyses and to estimate volumes of rock avalanches. Pre- and post-failure topographic surfaces were created from the DEM, and volumes were obtained by differencing the surfaces. Important constraints on the pre-failure surface include distinct scarp morphologies, topographic edges, rivers, mean slope orientation, and mean slope

Please cite this article as: Schleier, M., et al., Subaqueous rock-avalanche deposits exposed by post-glacial isostatic rebound, Innfjorddalen, Western Norway, Geomorphology (2016), http://dx.doi.org/10.1016/j.geomorph.2016.08.024

gradient. Additionally, field estimates of deposit thickness were multiplied by the spatial extent of mapped deposits to estimate bulked volumes. The initial rock volume was estimated by applying a bulking factor of 0.25 (i.e., 25% volume increase due to fragmentation), as proposed, for instance, by Hungr and Evans (2004) and Boultbee et al. (2006). The former authors quote a typical range of 18–35% and other authors report similar values (Dunning et al., 2007; Evans et al., 2009; Pirulli, 2009; Welkner et al., 2010).

3.4. Surface-exposure dating

Surface-exposure dating using the in-situ terrestrial cosmogenic nuclide (TCN) ^{10}Be was conducted to obtain absolute ages for the different rock-avalanche deposits in Innfjorddalen Valley. Gosse and Phillips (2001) summarize the method and Ballantyne et al. (1998), Hermanns et al. (2001, 2004) and Ivy-Ochs et al. (2009) offer examples of applications to landslide research. Nine samples were collected in 2011 from four different deposits following the sampling protocol in Blais-Stevens et al. (2011) and Hermanns et al. (2012b). Samples were collected from at least two independent rock boulders on the surface of each deposit, where possible from quartz veins. Sample preparation, analysis and age calculation were done at the Dalhousie University Geochronology Centre in Halifax, Canada. AMS analyses were performed at Lawrence Livermore National Lab, Livermore, USA (CAMS-LLNL). Ages were determined using the CRONUS calculator on the KU server, version 1.0 (Borchers et al., 2016), with ^{10}Be production systematics as

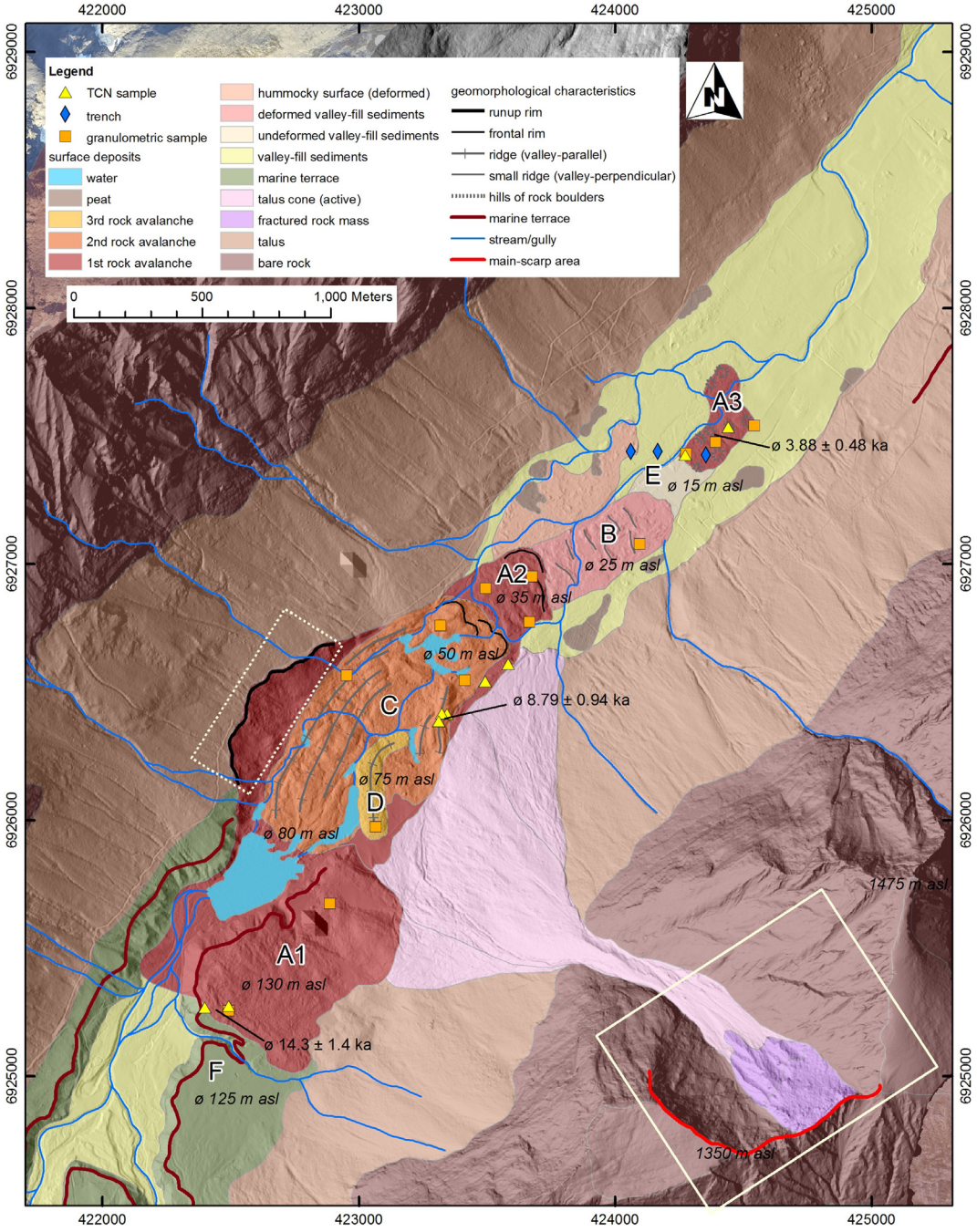

Fig. 3. Distribution of rock avalanche and other deposits in Innfjorddalen Valley, geomorphological characteristics, mean elevations, and sample locations. Areas for granulometric description are labeled A to D. The rock-avalanche source area on Gråfonnfjellet Mountain is outlined by the solid white rectangle (main scarp at about 1350 m a.s.l.). The run-up area of the first rock avalanche is indicated by the dotted white rectangle. (Coordinate system: WGS1984, UTM Zone 32N.)

Please cite this article as: Schleier, M., et al., Subaqueous rock-avalanche deposits exposed by post-glacial isostatic rebound, Innfjorddalen, Western Norway, Geomorphology (2016), http://dx.doi.org/10.1016/j.geomorph.2016.08.024

described in Lifton et al. (2014). The samples supplement a single sample collected in the year 2003 from the stratigraphically highest rock-avalanche deposit. This sample was prepared and analyzed at GeoForschungsZentrum (GFZ) Potsdam, Germany and Labor für Ionenstrahlphysik (LIP), ETH Zurich, Switzerland. Its age was determined in the same way as the other nine samples.

3.5. Dynamic runout analyses

Dynamic runout modeling using the software code DAN3D (McDougall and Hungr, 2004; McDougall, 2006; Hungr and McDougall, 2009) was carried out to analyze the runout of the rock avalanches as a test of the reliability of landform interpretation. Runout path topography and initial volume were input into the models. The distribution of different materials along the runout path was derived from field mapping. To determine the most reliable model, several DAN3D models were run with different values for input variables (e.g., Voellmy rheology with friction coefficient and turbulence coefficient ranging between 0–0.15 and 400–1000 m/s^2, respectively). The model results were compared with the spatial extent of the rock-avalanche deposits. To compare and verify modeling results and field mapping, the velocity was calculated for one rock avalanche based on its run-up height (Crandell and Fahnestock, 1965). Fahrböschung angles (Heim, 1932) were determined for all deposits based on the mapping and modeling results.

4. Geomorphology, stratigraphy and chronology of rock avalanches

4.1. Spatial distribution and characteristics of surface deposits

Deposits of several rock avalanches are preserved on the Innfjorddalen valley floor (Seljesæter, 2010; Schleier et al., 2013). The deposits overlie each other, thus providing a measure of their relative timing. Three main rock avalanche events are distinguished from the spatial distribution and characteristics of the deposits. At least one event created a dam that impounded a lake.

The rock-avalanche deposits cover an area of about 1.44 km^2 (Figs. 3, 4 and 5, and Table 1). The first and stratigraphically lowest rock-avalanche deposit is continuous and is labeled A1 and A2. It is separated from an isolated rock-boulder deposit (A3) by deformed (B) and undeformed (E) valley-fill sediments. The second rock-avalanche deposit (C) overlies the first deposit (A1 and A2) and has a smaller extent. The third and stratigraphically highest rock-avalanche deposit (D) is much smaller than the deposits of the earlier rock avalanches and lies on top of them. The rock-avalanche deposits overlie talus, valley-fill sediments, and a marine terrace (F). The source of all three rock avalanches a large niche at Gråfonnfjellet Mountain.

Figs. 6 and 7 summarize results of granulometric analyses on samples collected from the rock-avalanche deposits (A–D, Fig. 3), and Table 1 summarizes extent, thickness and volumes of rock-avalanche deposits.

4.1.1. First rock-avalanche deposit (A1 and A2)

The first and largest of the rock-avalanche deposits is a continuous rock-boulder deposit that covers an area of 1.44 km^2 and has an estimated bulked volume of about 20.6 × 10^6 m^3 (A1 and A2 in Figs. 3 and 4, and Table 1). The deposit is up to 800 m wide and extends about a length of 2200 m on the valley floor. The deposit has a lobate form, longitudinal ridges and a run-up on the opposite valley slope of about 100 m (Figs. 3 and 4). The deposit comprises features A1 and A2, which are a carapace of rock boulders with similar grain size and roundness characteristics (Figs. 6 and 7). The deposit supports a relatively dense birch forest, but lacks a conspicuous soil. The boulders have a moss cover of varying thickness (about 5–10 cm). The proximal part of the deposit lies 130 m a.s.l., whereas the distal part extends down to 35 m a.s.l. The deposit is partly covered by younger rock-avalanche deposits C and D which is evident from geomorphological relations.

Deposit A1 lies on a marine-terrace (F), which can be traced into the inner part of the valley (Figs. 3 and 4). No soil material was found at the

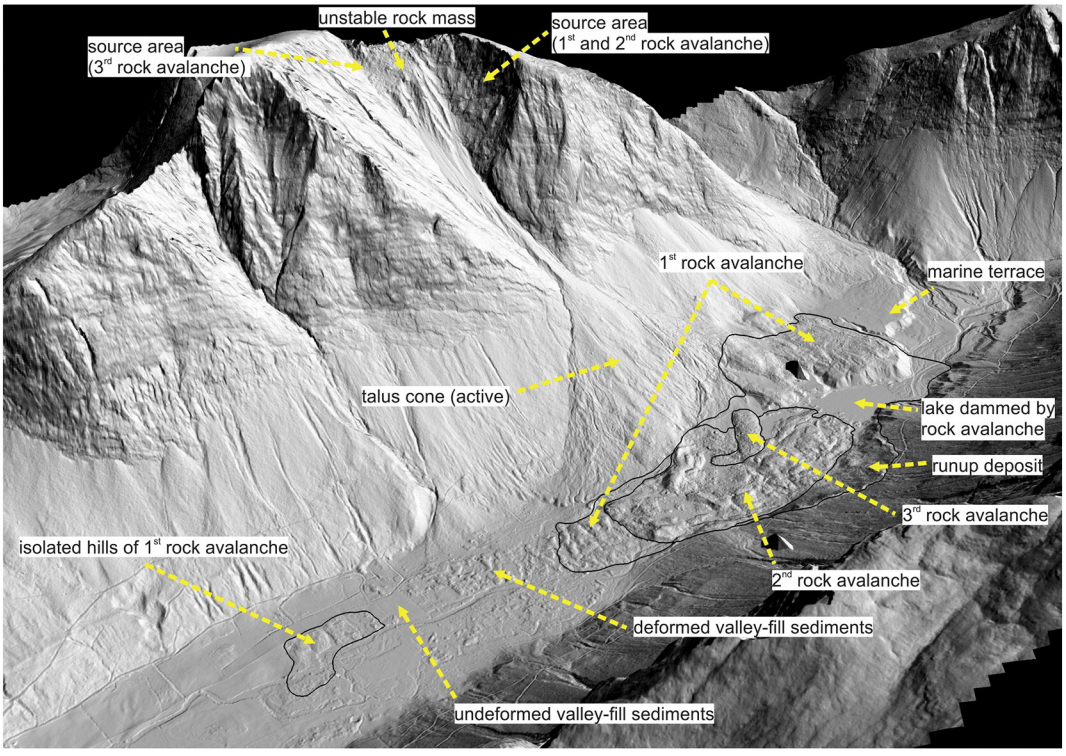

Fig. 4. Shaded-relief, oblique view of the study area (view towards SSE). The main geomorphological features are named (see text for detailed descriptions), and the spatial extent of the rock-avalanche deposits is outlined by black lines. Refer to Figs. 2 and 3 for scale.

Please cite this article as: Schleier, M., et al., Subaqueous rock-avalanche deposits exposed by post-glacial isostatic rebound, Innfjorddalen, Western Norway, Geomorphology (2016), http://dx.doi.org/10.1016/j.geomorph.2016.08.024

contact between the deposit A1 and the terrace surface. This terrace is characterized morphologically by a distinct edge and a 30-m-high step down to valley floor. An exposure in this embankment reveals graded bedding of sand and gravel inclined 25° towards the N, and showing foreset and onset structures (Fig. 8c).

4.1.2. Isolated hills of rock-avalanche debris (A3)

Isolated, nearly concentric hills of rock-avalanche debris up to 3 m high separated from deposit A2 by valley-fill deposits B and E at an elevation of 15 m a.s.l. The hills have a carapace of large rock boulders and cover a total area of 61×10^3 m^2 (Figs. 3, 4 and 8, Table 1). Assuming a mean thickness of 5 m, the total bulked volume of the rock-avalanche debris in the hills is estimated to be 0.3×10^6 m^3. The granulometric characteristics of the debris, summarized in Figs. 6 and 7, are similar to those of A1, A2 and B but with fewer large boulders. The vegetation on the hills is similar to that on deposits A1 and A2, except that it is less dense and with a moss-cover thickness of about 10 cm. The GPR profile over deposit A3 shows m-sized hill-like convex structures to about 4 m depth with intervening sub-horizontal layers (Fig. 9c). Beyond the most distal hill, the profile shows sub-horizontal to gently and partly undulating reflectors with no any hill-like structures (Fig. 9).

4.1.3. Deformed and undeformed valley-fill sediments (B and E)

Deposit A3 is separated from deposits A1 and A2 by deformed (B) and undeformed (E) valley-fill sediments (Figs. 3 and 4). The deformed sediments lie at elevations of 20–30 m a.s.l. adjacent to deposit A2. Further downvalley are apparently undeformed sediments below 20 m a.s.l. Deposit B underlies an undulated surface with small elongate depressions and ridges that are perpendicular to the valley axis. The deposit is characterized in the GPR profile by irregular undulating reflectors and small depressions and ridges to a depth of about 8 m (Fig. 9a). Although no continuous rock-boulder deposit was found at the surface, there are some isolated boulders (see Figs. 6 and 7 for granulometric characteristics).

The area between rock-avalanche deposit A3 and deformed sediments B is underlain by valley-fill deposit E. The surface is relatively flat and even and thus does not exhibit any deformation. It has a mean elevation of about 15 m a.s.l. No rock boulders are present within this area (Fig. 8). The GPR profile shows regular sub-horizontal reflectors to a depth of 5 m (Fig. 9b).

A trench was dug within deposit B and another at the presumed transition between deposits B and E (Figs. 3 and 10). No real difference is observed between the trenches. Both trenches exposed massive sand and gravel of fluvial or marine origin, but with lack of any lamination. Clasts and lenses of rock-avalanche material or laminated fine-grained sediments are present within the deposit.

Another trench was opened in deposit A3 in the year 1997 by L.H. Blikra (unpublished dataset). The trenched sediments were described as a succession of fluvial or marine gravel and peat that had been deformed by, and mixed with rock-avalanche debris.

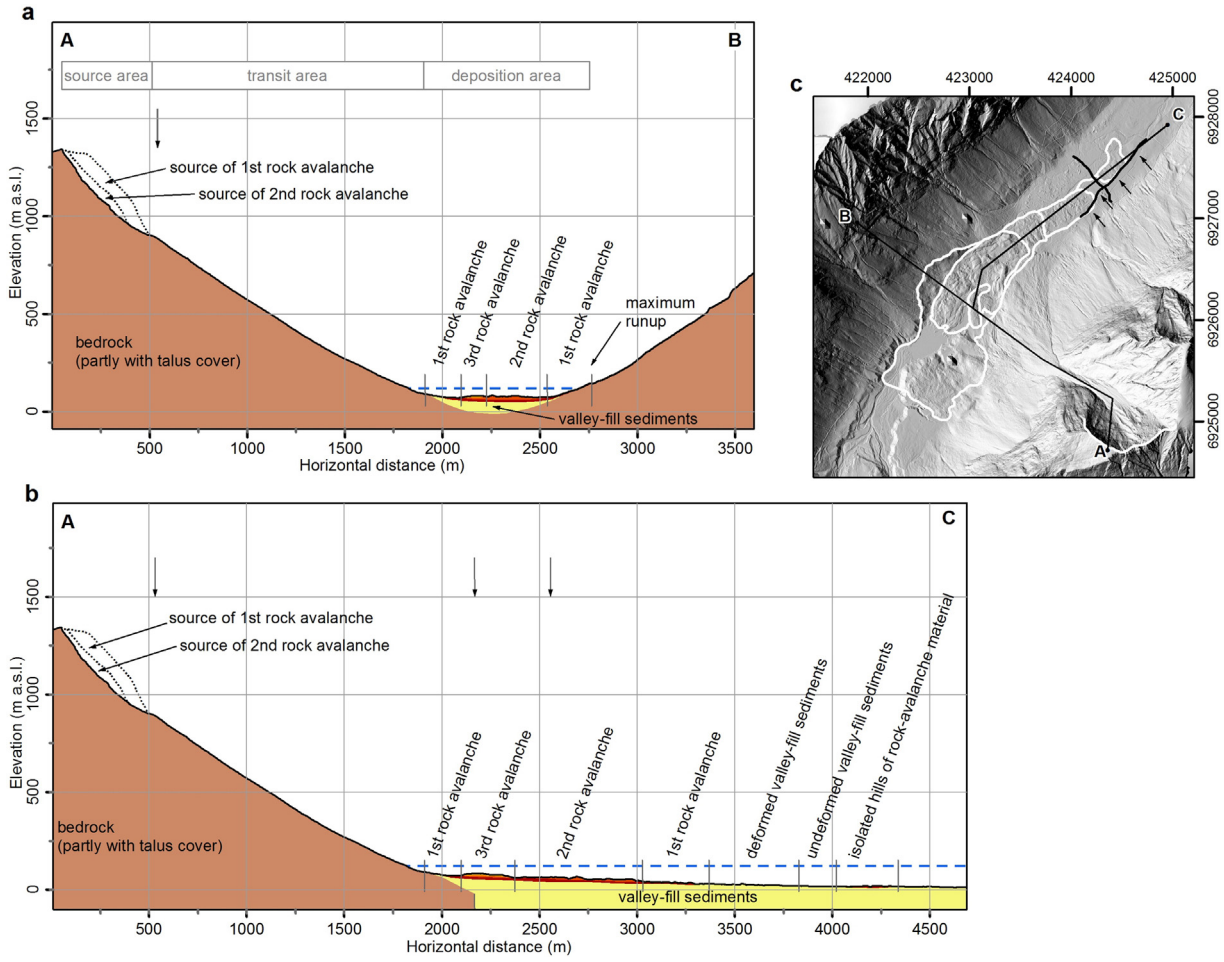

Fig. 5. Topographic profiles in Innfjorddalen Valley. (a) Transverse profile A-B and (b) longitudinal profile A-C showing the distribution of rock-avalanche deposits and the marine limit (horizontal dashed line). Black arrows mark changes in slope along the profile. (c) Hillshade map showing the locations of topographic profiles (A-B and A-C, black lines) and GPR profiles (thick black lines). Black arrows along the GPR profile mark locations of sections presented in Fig. 9. Spatial extents of the deposits of the rock avalanches are indicated by white solid lines (refer to Fig. 3 for a detailed description).

Please cite this article as: Schleier, M., et al., Subaqueous rock-avalanche deposits exposed by post-glacial isostatic rebound, Innfjorddalen, Western Norway, Geomorphology (2016), http://dx.doi.org/10.1016/j.geomorph.2016.08.024

Table 1
Estimated thickness, mapped spatial extent and calculated and modeled volume of rock-avalanche deposits.

Deposit		Mapped spatial extent	Field estimated mean thickness	Volume		
		Bulked	Initial			DAN3D
		(10^3 m^2)	(m)	(10^6 m^3)	(10^6 m^3)	(10^6 m^3)
1st rock avalanche	Continuous	1376	15	20.6	16.5	15.1
	Isolated hills	61	5	0.3	0.2	
2nd rock avalanche		523	12	6.3	5.0	5.4
3rd rock avalanche		44	8	0.4	0.3	0.3
Total		–	–	27.6	22.0	20.8

Notes: Area of first rock avalanche includes also the areas of the second and third events (areas A1, A2, C, D, Fig. 3). Area of second rock avalanche includes also the area of the third event (areas C, D). Bulked volume was calculated from area and field-estimated thickness. The source rock volume was then calculated using a bulking factor of 25%.

4.1.4. Second rock-avalanche deposit (C)

A stratigraphically younger rock-avalanche (C) covers an area of 523×10^3 m^2 on the valley floor between 50 and 80 m a.s.l and has an estimated bulked volume of 6.3×10^6 m^3 (Figs. 3 and 4, Table 1). The material overlies and is confined to the continuous deposit A1 and A2, is lobate and has large longitudinal ridges. This rock-avalanche formed a dam and impounded a lake that has persisted in a smaller form to the present. The deposit is capped by a carapace of rock boulders (see Figs. 6 and 7 for granulometric characteristics). The rock boulders are more angular and lie less tight than those on the surface of deposits A1 and A2, and more often have a 'jigsaw' structure (i.e., rock fragments originating from the same boulder lying closely together with an interlocking jigsaw structure). The deposit is less dense vegetated than those of A1 and A2, with chiefly coniferous forest. Deposit C is partly covered by the third rock-avalanche deposit (D).

4.1.5. Third rock-avalanche deposit (D)

The deposit of the third rock avalanche (D) is stratigraphically the highest and is also the smallest of the three. It covers an area of 44×10^3 m^2, contains an estimated bulked volume of 0.4×10^6 m^3 and lies on top of deposits A1 and C at a mean elevation of 75 m a.s.l. (Figs. 3 and 4, Table 1). The deposit has a characteristic compact carapace of rock boulders similar to the other rock-avalanche deposits. However, the boulder size and roundness differ from those of the other deposits (Figs. 6 and 7). Fine-grained material is less abundant, jigsaw boulders are common and boulders are angular. The deposit lacks a forest cover, and has at most only patchy, a thin moss vegetation.

4.2. Source of the rock avalanches

The source of the three rock avalanches is located in a large niche on the NW-facing slope of Gråfonnfjellet Mountain on the west side of the valley (Figs. 3, 4 and 8). The niche is formed from three main slope faces (orientations in dip direction/dip), one NE-facing (060/50), another NW-facing (310/70) and a third W-facing (260/45). Based on the DEMs, the whole niche represents a volume of approximately 47×10^6 m^3 of absent rock mass. Different source areas for the three

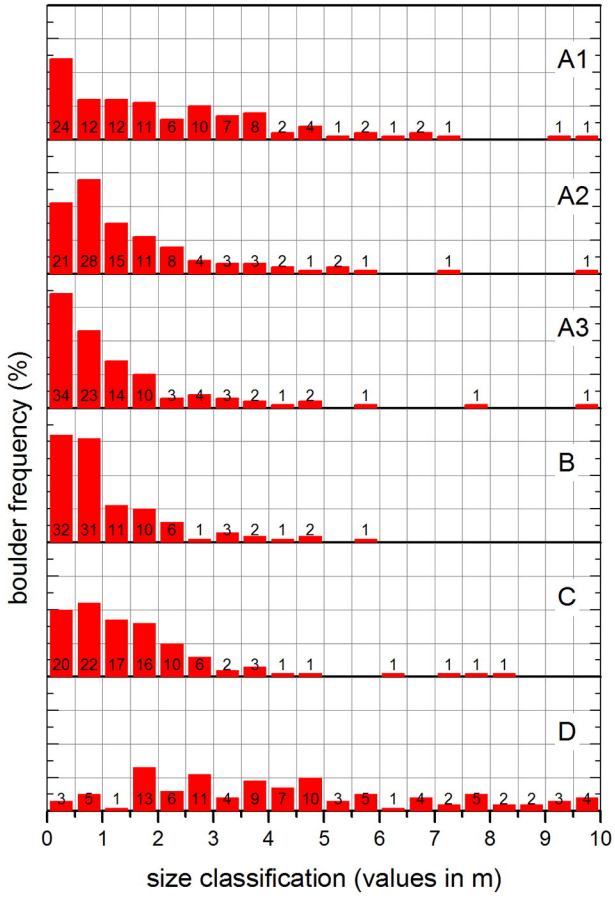

Fig. 6. Boulder size distribution for the deposits A to D (see Fig. 3 for locations). The horizontal grid lines mark 10% intervals.

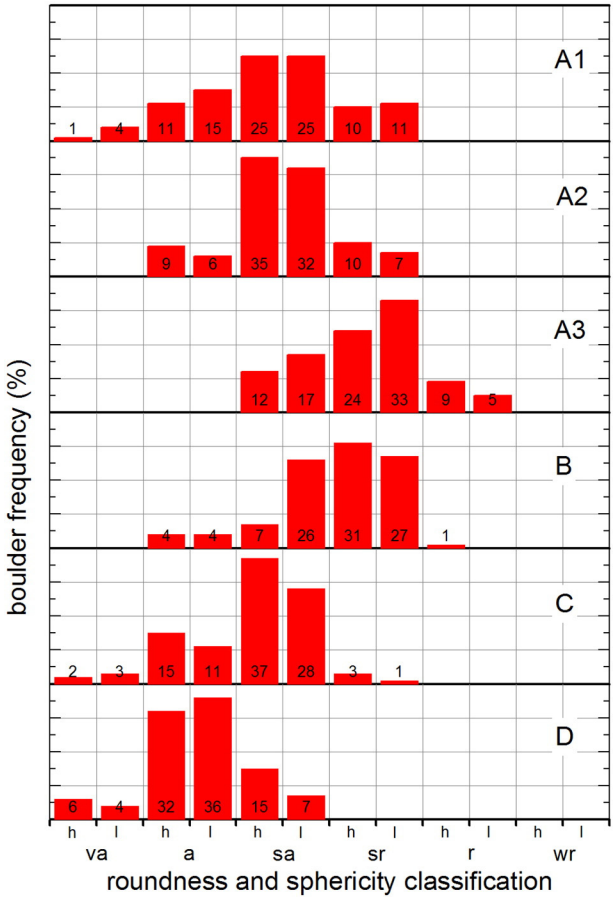

Fig. 7. Boulder roundness and sphericity for the deposits A to D (see Fig. 3 for locations; va, very angular; a, angular; sa, sub-angular; sr, sub-rounded; r, rounded; wr, well rounded; h, high sphericity; l, low sphericity). The horizontal grid lines mark 10% intervals.

Please cite this article as: Schleier, M., et al., Subaqueous rock-avalanche deposits exposed by post-glacial isostatic rebound, Innfjorddalen, Western Norway, Geomorphology (2016), http://dx.doi.org/10.1016/j.geomorph.2016.08.024

rock avalanches within this niche were identified based on field observations, helicopter reconnaissance, and photo and DEM interpretations. A large distinct scarp is evident on the NE-facing slope of the niche and a smaller scarp is present on the SW-facing slope (Fig. 8). The former is thought to be the source of the first and second rock avalanches, and the latter the third rock avalanche.

Additionally, an unstable rock mass of about 1.8×10^6 m^3 in volume is present in the upper part of the central, W-facing slope of the niche. It is one of >250 unstable rock slopes identified in Norway to date (Oppikofer et al., 2015). A large talus cone has formed in the lower part of the niche and along the former paths of the rock avalanches. It remains a locus of rock falls, debris flows, snow avalanches and gully erosion (Fig. 8).

4.3. Ages of the rock-avalanche deposits

Each rock-avalanche deposit was dated using the ^{10}Be TCN technique (Fig. 3, Table 2). The apparent ages of the three rock avalanches, from oldest to youngest, are 14.3 ± 1.4 ka, 8.79 ± 0.94 ka, and 1.028 ± 0.380 ka. A historic rock avalanche is mentioned in church books from the year 1611–12 CE (i.e., historic chronicle of the archive of the local Christian church). It caused the death of farmers who suffocated in the dust cloud (Furseth, 2006). A sample from an isolated hill of rock-avalanche debris (A3) returned an age of 3.88 ± 0.48 ka. This TCN age is consistent with a radiocarbon age on plant detritus recovered from a trench in the area of the isolated hills by Blikra in 1997 (Blikra et al., 2002). Two samples (INF-05 and INF-09) were not analyzed because of insufficient quartz for an age determination and two others (INF-04 and INF-08) also showed difficulties due to less quartz content and too high Al content.

5. Discussion of geomorphological evidences

5.1. Volumes of deposits and source area

The deposits of the three identified rock avalanches have a field-estimated total bulked volume of 27.6×10^6 m^3. Taking into consideration a bulking factor of 0.25, the bulked volume corresponds to an initial rock volume of 22×10^6 m^3, which is consistent with the estimate of the missing rock of the identified three source areas derived by topographic modeling (Fig. 8, Table 1). However, volume estimates based on preserved deposits are only approximate and have large uncertainties stemming from uncertain deposit thicknesses, material entrainment, bulking, and post-depositional erosion (Hermanns et al., 2014). Especially erosion and material entrainment are quite complex phenomena in rock-avalanche propagation and strongly affect the runout behavior (Hungr and Evans, 2004; McDougall and Hungr, 2005; Crosta et al., 2009a; Evans et al., 2009; Luna et al., 2012).

A total rock mass of about 47×10^6 m^3 is missing from the whole large niche that is thought to include the sources of the three rock avalanches documented in this paper. This volume is nearly twice the estimate of the total initial volume of the rock-avalanche deposits. Hence,

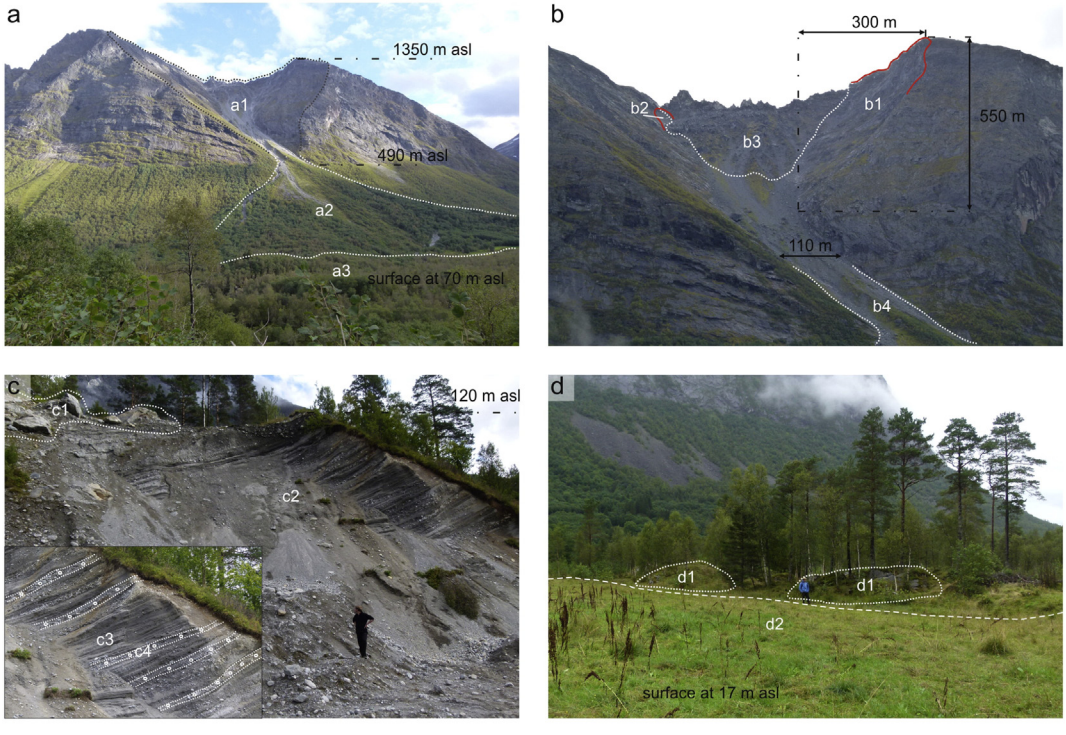

Legend of marked areas

a1: main niche of source area
a2: rock-avalanche path and active talus cone
a3: rock-avalanche deposits
b1: source area of 1st and 2nd rock avalanches
b2: source area of 3rd rock avalanche
b3: unstable rock mass
b4: path (active)

c1: rock-avalanche deposit (on marine terrace)
c2: marine terrace (delta deposits)
c3: layered sand and silt
c4: layered gravel
d1: isolated hills of rock-avalanche material
d2: undeformed valley-fill sediments

Fig. 8. Photographs of the main geomorphological features in Innfjorddalen Valley. Geomorphological features are outlined by white dotted lines, and abbreviations are summarized in the legend. For scale, refer to Figs. 2 and 3. (a) Gråfonnfjellet Mountain (view towards SE), showing source, path and part of the deposition area of the rock avalanches. (b) Closer view of the source area showing the main scarps of rock avalanches (red lines) and the remaining unstable rock mass. (c) Exposure through marine-terrace deposit on the valley floor (view towards SSE) showing rock-avalanche material lying on top of the foreset beds of a delta at about 120 m a.s.l. (upper left). Small inset provides a closer view of the typical bedding structures of a propagating delta (modified from Schleier et al., 2013). (d) Isolated hills of rock-avalanche debris (view towards NNE) at their boundary with the undeformed valley-fill sediments (modified from Schleier et al., 2013).

Please cite this article as: Schleier, M., et al., Subaqueous rock-avalanche deposits exposed by post-glacial isostatic rebound, Innfjorddalen, Western Norway, Geomorphology (2016), http://dx.doi.org/10.1016/j.geomorph.2016.08.024

an additional rock mass of about 25×10^6 m^3 is missing from the niche. Two possible explanations for this discrepancy are as follows. Several large rock avalanches prior to or during the Late Pleistocene glaciations may have sources in the same niche, but their deposits have been eroded or moved downvalley by glacier ice. Or alternatively, thick younger valley-fill sediments may cover these old rock-avalanche deposits, which are thus not visible in the GPR profile (Fig. 9). The first of the three rock avalanches that have been documented fell onto soft fjord sediments. It is possible that part of the rock-avalanche debris subsided into these sediments and thus are not visible at the surface. Such a scenario would lead to an underestimation of the observed deposit volume. However, such deposits are not visible in the GPR profile or in the trenches (Figs. 9 and 10), which would be very unlikely for such a large volume.

The unstable rock mass remaining in the niche (Figs. 3 and 8) and the active debris cone below it indicate that rock-slope failures are frequent at this site. Multiple failures in the same source area support a hypothesis that rock-slope failures can, in some instances, increase the probability of future failures due to accelerated decompression (Hermanns et al., 2006) or simply because of unstable material remains on the rock slope.

5.2. ^{10}Be surface-exposure ages

Some of the ^{10}Be ages on the same rock-avalanche deposit are significantly different (Table 2), requiring comment. Samples INF-06 and INF-07 were collected from the deposit of the first rock avalanche. INF-07 (14.3 ± 1.4 ka) was the priority sample because the boulder surface

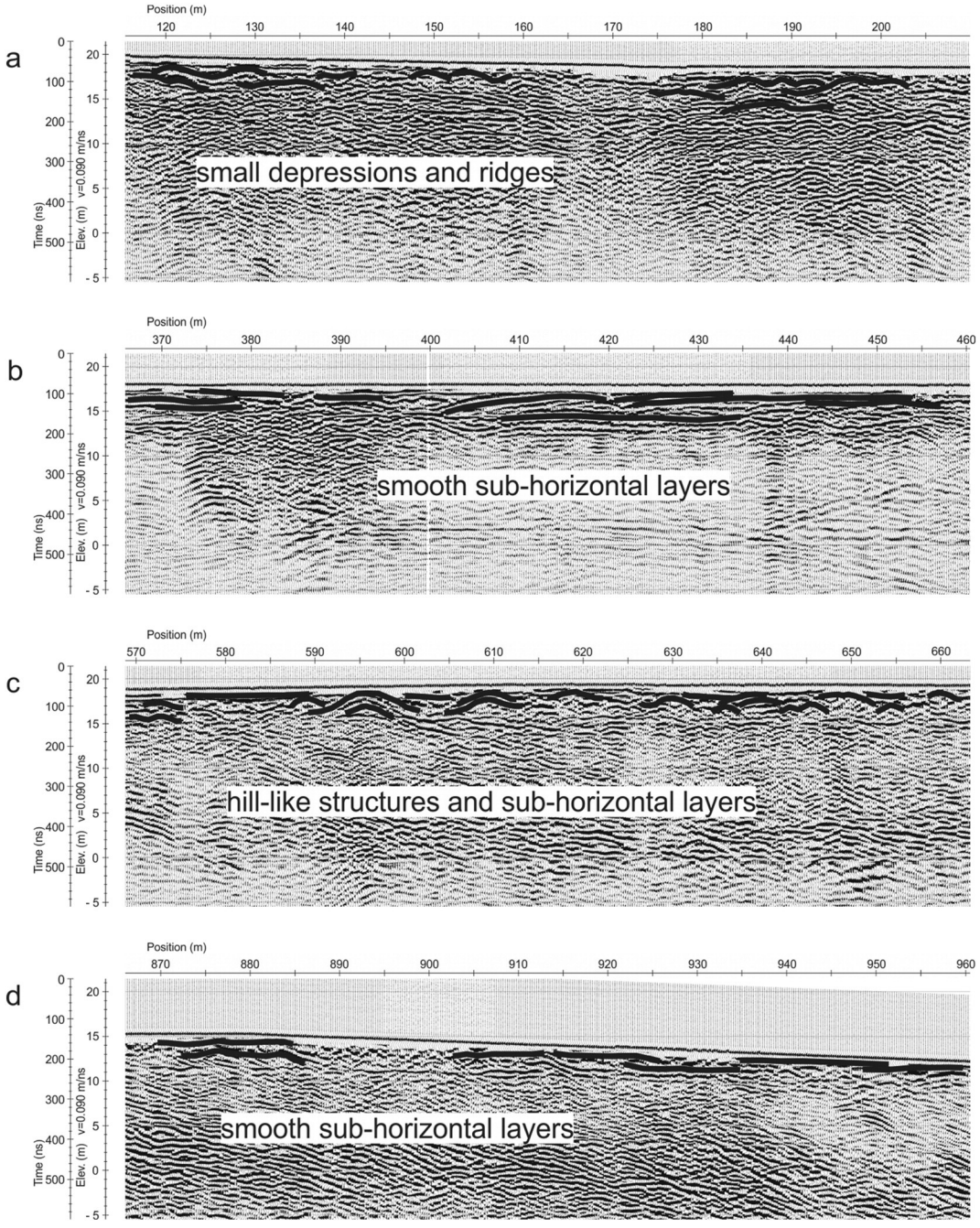

Fig. 9. Four representative sections of the valley-parallel GPR profile (see Fig. 5c for location): (a) deformed valley-fill sediments, (b) undeformed valley-fill sediments, (c) isolated hills of rock-avalanche debris, and (d) valley-fill sediments beyond the distal limit of rock-avalanche deposits (sections extracted from NGU, 2009).

Please cite this article as: Schleier, M., et al., Subaqueous rock-avalanche deposits exposed by post-glacial isostatic rebound, Innfjorddalen, Western Norway, Geomorphology (2016), http://dx.doi.org/10.1016/j.geomorph.2016.08.024

was flat and there is no possibility that the boulder had moved since emplacement. In contrast, because of lack of alternative good quartz samples, sample INF-06 was collected from a boulder that shows higher possibility that it may have moved after emplacement and may have suffered from erosion. The calculated age has a higher uncertainty and thus it is considered less reliable. Samples INF-04 and INF-08 gave similar ages, which are close to the time of the inferred date of the third rock avalanche, but both ages should be interpreted carefully and results should not be unequivocally accepted. There were problems during analyses, and the amount of beryllium in the samples was very low, with the result that the uncertainties in the ages are high, 36.2 and 21.2%, respectively. Furthermore, the sampled boulders are close to the margin of the deposit, on the side facing the active talus cone, thus the ages could be displaced or even deposited by the third rock avalanche. INF-03 (8.79 ± 0.94 ka) is considered an accurate age for the second rock avalanche. Sample R120803-03 was collected from the surface of the third rock avalanche, and its age is slightly too old considering the date inferred from the church books, although it does overlap the inferred 1611–12 CE if the large uncertainty in the TCN age (36.9%) is taken into account. However, it is by far the smallest of the three rock avalanches, and hence inheritance of beryllium on the sampled rock-boulder face is possible. Samples INF-01 and INF-02 are in agreement and have a mean value of 3.88 ± 0.48 ka.

5.3. Entry of the first rock avalanche into a shallow fjord

A rock avalanche about 15.1 × 10^6 m^3 in volume (initial, model) happened 14.3 ± 1.4 ka ago (Figs. 3 and 8). The spatial distribution, geomorphic characteristics and age of the deposit suggest that the rock avalanche struck the floor of a shallow fjord at Innfjorddalen. The complex deposits are now exposed due to post-glacial isostatic uplift.

Deposits A1 and A2 have the typical characteristics of rock-avalanche material, including a carapace of large, mainly sub-angular and angular rock boulders (Hewitt, 2009b; Dunning and Armitage, 2011). Its high mobility, indicated by run-up on the opposite slope, frontal rims and longitudinal ridges (Figs. 3 and 4) is also evidence of rock avalanching (Evans et al., 1989; Erismann and Abele, 2001; Legros, 2002; Poschinger, 2002; Dufresne and Davies, 2009).

No soil material was found at the contact between deposit A1 and the marine terrace F on which it lies (Figs. 3 and 8), which could indicate that the surface was not subaerial when the rock avalanche occurred. Deposit F is interpreted to be formed by a propagating marine delta that was at sea level at the time the rock avalanche happened. Today, this surface is 120 m a.s.l., which indicates at least this amount of uplift due to postglacial isostatic rebound.

These findings, together with the TCN age of 14.3 ± 1.4 ka and research on the marine limits (Hansen et al., 2014; NGU, 2015), indicate that the first rock avalanche entered the shallow fjord and probably generated a displacement wave. It is inferred that rock-avalanche debris was then at least partly deposited approximately 70 m below the sea surface (Fig. 5).

The deposit of the first rock avalanche spans the entire width of the valley and, although it has been modified and partly covered by younger rock-avalanche deposits, it likely formed a dam that impounded a lake or at least bisected the shallow fjord. However, no associated lacustrine sediments were found, probably because the deposits are buried beneath the younger rock-avalanche deposits.

Although composed of similar material, the isolated hills of rock-avalanche debris and the deformed and undeformed valley-fill sediments between these hills and the continuous rock-avalanche deposit require discussion.

It is hypothesized that the hills were emplaced by the first rock avalanche as tomas per Abele (1974) and Poschinger (2002). Other explanations for those isolated hills, including isolation by fluvial erosion, deposition controlled by dead ice in the valley, glacier advance across a rock-avalanche deposit, or deposition on water-saturated alluvial

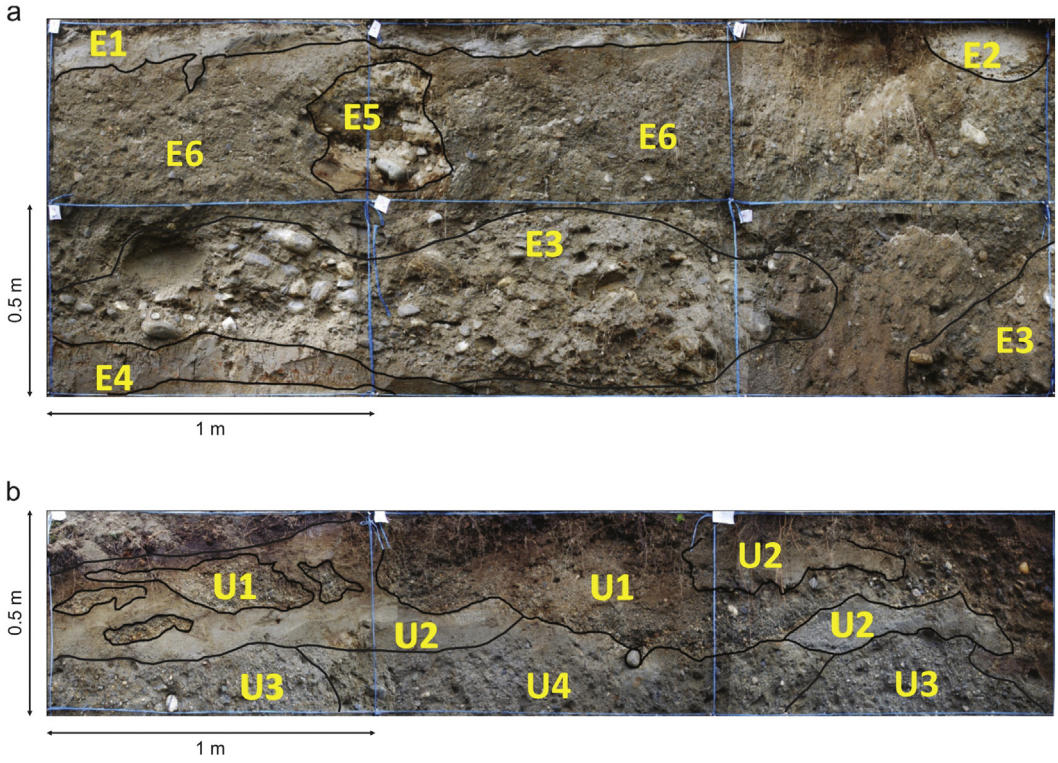

Fig. 10. Photographs of the walls of two trenches in deformed and undeformed valley-fill sediments (modified from Seljesæter, 2010, and Schleier et al., 2013, see Fig. 3 for location). (a) Eastern trench with five deformed units (E1, E2: laminated fine silt and clay mixed with sand; E3, E5: pockets of massive gravel within massive sand; E4: laminated clay and fine sand; E6 massive sand). (b) Western trench with three deformed units (U1: coarse iron-stained sand; U2: iron stained fine sand and clay; U3: massive gravel similar to unit E3 from the eastern trench; U4: massive sand).

Please cite this article as: Schleier, M., et al., Subaqueous rock-avalanche deposits exposed by post-glacial isostatic rebound, Innfjorddalen, Western Norway, Geomorphology (2016), http://dx.doi.org/10.1016/j.geomorph.2016.08.024

Table 2
^{10}Be surface-exposure ages of samples of rock-avalanche deposits in Innfjorddalen Valley.

Description	Sample	Latitude (°)	Longitude (°)	Elevation (m a.s.l.)	^{10}Be age $\varepsilon = 0$ mm ka^{-1} (ka)	Ext. unc. (1σ ka)	CV (%)	Other ages
1st rock avalanche (continuous deposit; A1)	INF-06	62.450563	7.497813	130	5.06	0.62	12.3	
	INF-07	62.450500	7.496071	125	14.3	1.4	9.8	
1st rock avalanche (central deposit; A2)	INF-08	62.462778	7.518413	50	0.565	0.12	21.2	
	INF-09	62.462149	7.516718	55	n.n.	n.n.	n.n.	
1st rock avalanche (isolated hills; A3)	INF-01	62.470232	7.531426	20	3.91	0.45	11.5	3800 cal yr BP (^{14}C age, Blikra et al., 2002)
	INF-02	62.471235	7.534635	20	3.85	0.51	13.2	
2nd rock avalanche (C)	INF-03	62.460970	7.513868	70	8.79	0.94	10.7	
	INF-04	62.460993	7.513479	75	0.525	0.19	36.2	
	INF-05	62.460712	7.513241	70	n.n.	n.n.	n.n.	
3rd rock avalanche (D) (sampled 2003)	R120803-03	62.4622	7.5131	93	1.028	0.380	36.9	1611–12 CE (church book, Furseth, 2006)

Notes: ε is the erosion rate, σ is the standard deviation, and CV is the coefficient of variation. Sample locations are shown in Fig. 3.

sediments seem unlikely (Abele, 1974, 1991; Erismann and Abele, 2001; Poschinger, 2002; Poschinger et al., 2006; Poschinger and Kippel, 2009).

Rather, the hills are large fragments of rock-avalanche material that separated from the main mass of the rock avalanche and ran across water-saturated sediments on the floor of the shallow fjord. Poschinger (2002) argues that undrained loading by the rock-avalanche facilitates the transport of tomas far beyond the limit of the main deposit. As the spatial distribution of the deposits indicates, primary the underlying sediments must have been water-saturated.

Other deposits associated with this re-sedimentation of alluvium are the Bonaduz gravel associated with the Flims rockslide and described by Abele (1991), Poschinger (2002) and Poschinger et al. (2006), which are located between tomas and main landslide deposit. The Bonaduz gravel is composed of gravelly sand and containing clasts of laminated lacustrine sediments and includes ubiquitous subvertical dewatering structures. The deformed valley-fill sediments B in Innfjorddalen may represent similar deposits. The GPR profile (Fig. 9) shows deformation, and trenches (Fig. 10) reveal mixed sediments, including pockets of gravel floating within massive sandy sediments.

The isolated hills of rock-avalanche debris were deposited on the paleo-seafloor, thus one might argue that the apparently undeformed valley-fill sediments E were deposited by marine and fluvial processes after the rock avalanche occurred. No cover of fine-grained laminated sediments, however, was found in the trenches. This is not unexpected as there was likely a rock-avalanche dam farther up the valley that restricted sediment delivery down-fjord. Furthermore, it is likely that coastal processes (e.g., wave, currents) and later fluvial processes affected the rock-avalanche deposits after their emplacement. The slightly higher percentage of sub-rounded and rounded boulders in the isolated hills deposit A3 compared to deposits A1 and A2 (Figs. 6 and 7) may reflect this reworking.

It might seem possible that the deposits of the first rock avalanche form a single continuous deposit, in which case the isolated hills of rock-avalanche debris and the main rock-avalanche deposit are connected in the subsurface and this connection is not visible at the surface because of the fluvial sediment cover. However, this interpretation is not plausible for Innfjorddalen, because such sediments are visible in the GPR profile and the trenches (Figs. 9 and 10). The irregular hill-like convex structures in the GPR profile are rock boulders of the rock-avalanche debris, for instance, tomas. Coherent undulating reflectors represent the deformed valley-fill sediments, and smooth and flat sub-horizontal reflectors record the bedded undeformed valley-fill sediments.

The ^{10}Be surface-exposure ages of the first rock avalanche (14.3 ± 1.4 ka) differs from that of the isolated hills (mean value 3.88 ± 0.48 ka) (Fig. 3, Table 2). However, these ages are consistent with the presented interpretation of the sequence of events. Part of the rock avalanche entered the fjord and came to rest below sea level. This part of the rock-avalanche deposit was shielded from cosmic radiation, resulting in lower production of cosmogenic nuclides and therefore a younger exposure age than the true age of the rock avalanche. The surface-exposure age of the isolated boulders (3.88 ± 0.48 ka, now at 15 m a.s.l.) could represent the time when the deposit emerged from the sea because of postglacial isostatic uplift rather than the time of rock-avalanche deposition. There is some TCN production under water, but the amount is difficult to quantify. Isostatic rebound and therefore the relative fall in sea-level thus is not well dated in Innfjorddalen. Based on studies in other areas of Western Norway (Maiforth, 2010), sea level was about 25 m higher than today 3.0 ka ago. It is thus presumed that sea level in Innfjorddalen was tens of meters higher than today at about 3.9 ka ago and that the deposits were lifted out of water (about 15 m higher than today) somewhat later. It thus appears that post-depositional uplift of Innfjorddalen produced an apparent age difference of about 10.4 ka for deposits interpreted to be coeval.

5.4. Second and third rock avalanches

A second rock avalanche of about 5.4×10^6 m^3 (initial, model) and a third of about 0.3×10^6 m^3 (initial, model) occurred 8.79 ± 0.94 ka ago

Table 3
Rheologies assigned to travel-path materials used in the DAN3D models.

Rock-slope failure	Volume (10^6 m^3)	Travel-path material	Rheology	Unit weight (kN/m^3)	Friction angle (°)	Friction coefficient	Turbulence coefficient (m/s^2)	Internal friction angle (°)
1st rock avalanche	15.1	1) Talus	Voellmy	28	–	0.13	600	35
		2) Valley-fill sediments	Voellmy	28	–	0.09	700	35
		3) Water-saturated sediments	Voellmy	28	–	0.03	1000	35
2nd rock avalanche	5.4	1) Talus	Voellmy	28	–	0.10	600	35
		2) Rock-avalanche deposits	Voellmy	28	–	0.11	400	35
3rd rock avalanche	0.3	1) Talus	Frictional	28	25	–	–	35
		2) Rock-avalanche deposits	Frictional	28	33	–	–	35

Please cite this article as: Schleier, M., et al., Subaqueous rock-avalanche deposits exposed by post-glacial isostatic rebound, Innfjorddalen, Western Norway, Geomorphology (2016), http://dx.doi.org/10.1016/j.geomorph.2016.08.024

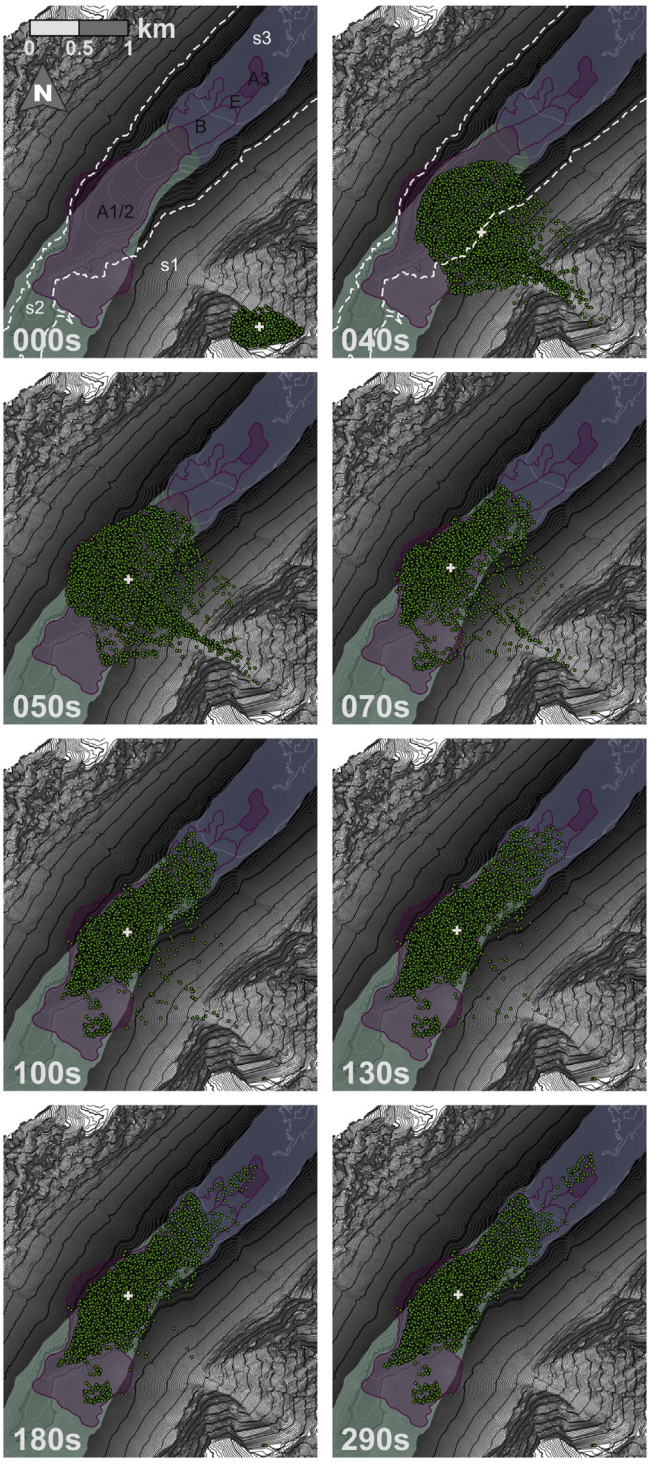

Fig. 11. Simulation of the first rock avalanche with DAN3D assuming two types of substrate. The propagation of the rock avalanche is shown in several time steps (times in seconds in the lower left corner) by the simulated particles (dots) and the center of gravity (cross). Contour interval is 25 m. Background color shows the substrate along the travel path (no color, s1: bedrock and talus; s2: valley-fill sediments; s3: water-saturated sediments) and the mapped extent of the deposits (hachured polygon, A1/2, A3: first rock avalanche; outlined polygon, B, E: deformed and undeformed valley-fill sediments). The white dashed line marks the approximate marine limit at 120 m a.s.l. after NGU, 2015. (For interpretation of the references to color in this figure legend, the reader is referred to the web version of this article.)

and 1.028 ± 0.380 ka, respectively (Figs. 3 and 8). The latter probably coincides with the historic event of the year 1611–12 CE.

Both rock avalanches left continuous deposits (C and D, Fig. 3) with carapaces of large mainly angular and sub-angular rock boulders, frontal rims, lateral levees and parallel ridges. The parallel ridges can be explained by internal differential shearing during the movement of the granular mass (Abele, 1974; Poschinger, 2002; Dufresne and Davies, 2009). However, movement might have been impeded by the underlying older rock-avalanche deposit, which represents an irregular and high friction surface.

The different rock-avalanche deposits were discriminated mainly by their geomorphology, granulometric characteristics and vegetation. There are distinct topographic steps (Fig. 5) and lobes (Fig. 3), especially in the frontal parts of the deposits. The third rock avalanche has larger and more angular boulders (Figs. 6 and 7) than the second rock avalanche, which also lie less tight. Differences in vegetation, from relatively dense deciduous forest (A1, A2 and A3) to less dense, more coniferous forest (C) and to nearly no vegetation (D), reflect the differences in ages of the deposits. However, there are no distinct soil layers at the stratigraphic contacts between the different deposits. This is perhaps not surprising because the oldest deposit A1 that is not covered by any younger deposit does not have a continuous soil cover—except for moss cover on boulders indicating that an exposure time of 14.3 ka is not long enough for soil development under the environmental conditions in this area.

The pronounced angularity of the rock boulders in the youngest rock-avalanche deposit supports the interpretation of a younger and less weathered deposit. The smaller extent of the deposits of the second and third rock avalanche and thus their higher Fahrböschung angles of 24° and 28°, respectively, indicate lower mobility that could have been

Table 4
Runout dynamics of the first, second, and third rock avalanches (ra) as simulated with DAN3D.

	1st ra (15.1×10^6 m^3)		2nd ra (5.4×10^6 m^3)		3rd ra (0.3×10^6 m^3)	
t	v max.	av. th.	v max.	av. th.	v max.	av. th.
(s)	(m/s)	(m)	(m/s)	(m)	(m/s)	(m)
0	0.0	48.3	0.0	36.6	0.0	10.5
10	209.9	25.2	140.2	17.8	54.0	6.0
20	119.4	13.4	101.9	9.6	74.3	3.0
30	89.2	9.9	81.4	6.6	83.6	1.3
40	74.5	7.6	55.8	4.7	78.2	0.6
50	53.1	6.4	37.3	4.0	76.3	0.4
60	38.0	7.0	28.0	3.8	76.5	0.5
70	35.7	7.8	24.1	3.8	74.3	0.7
80	27.0	8.0	23.0	4.0	73.7	1.0
90	22.5	8.4	18.9	4.2	72.4	1.5
100	20.4	8.6	16.8	4.5	71.5	2.1
110	17.5	8.7	15.7	4.7	42.6	2.3
120	14.3	8.8	14.0	4.9	1.0	2.4
130	14.4	8.9	12.6	5.0	–	–
140	15.4	8.9	15.4	5.2		
150	13.4	8.9	12.7	5.3		
160	12.8	9.0	–	–		
170	11.3	9.1				
180	12.1	9.3				
190	10.5	9.3				
200	10.3	9.4				
210	9.5	9.4				
220	8.9	9.5				
230	12.0	9.5				
240	10.8	9.5				
250	10.9	9.6				
260	9.8	9.6				
270	10.1	9.6				
280	10.3	9.7				
290	8.0	9.7				
300	9.9	9.7				
310	–	–				

Notes: The maximum velocity (v max.) and average thickness (av. th.) are shown for the modeled time steps (t).

Please cite this article as: Schleier, M., et al., Subaqueous rock-avalanche deposits exposed by post-glacial isostatic rebound, Innfjorddalen, Western Norway, Geomorphology (2016), http://dx.doi.org/10.1016/j.geomorph.2016.08.024

caused by the smaller volumes involved (Scheidegger, 1973) and the high-friction substrate along their travel paths, that are, older rock-avalanche deposits.

6. Dynamic modeling of rock-avalanche runout

6.1. First rock avalanche

The runout of a rock avalanche with an initial volume of 15.1×10^6 m^3 was modeled with DAN3D. The evidence presented in this paper suggests that the rock avalanche entered the fjord when relative sea level was about 120 m above the present datum (Fig. 5). Unfortunately, it is not possible with DAN3D to model rock-avalanche propagation within a water body.

Therefore, the model was stopped manually when the propagating mass reached 120 m a.s.l. This model assumes a different sea level at the time the rock avalanche occurred at an elevation of 20 m a.s.l. to account for an alternative hypothesis that is based solely on interpretation of the spatial distribution of the transition between the deformed (B) and undeformed (E) valley-fill sediments (Schleier et al., 2013). Thus, the rock avalanche propagated along the talus slope below Gråfonnfjellet Mountain into Innfjorddalen Valley and into the shallow fjord. Beyond the talus cone, the valley is floored by fine-grained water-saturated sediments. Thus, the modeling below the assumed water level is interpretive.

The applied model parameters are summarized in Table 3, and the modeling results are shown in Fig. 11 in the form of particle distribution at selected time steps. Table 4 summarizes the modeled maximum particle velocities and average thicknesses.

At 25 s the propagating rock-avalanche mass was still above the marine limit at an elevation of 120 m a.s.l. At 30 s it has past this elevation and at 40 s it has reached 60 m a.s.l. Thus the rock avalanche impacted the water body at about 30 s, at which time it generated a displacement wave. Thus the model was stopped at 30 s and the following comments are offered speculatively.

At 40 s the front of the rock avalanche arrived on the valley bottom with a mean velocity of about 44 m/s and started spreading up and down the valley. At 50 s the leading edge of the mass reached its maximum run-up height at the opposite slope and turned about 90° towards the NE, accompanied by a deceleration to <30 m/s. At 100 s the bulk of the rock-avalanche debris at the SW margin had come to rest, creating a dam. However, the mass was still moving over water-saturated sediments at its NE margin, and at about 130 s some material started to detach here from the main mass and moved in a rather isolated manner towards the NE (180 s) with comparatively low velocities (<10 m/s). All movement has ceased by 290 s.

The limit of the run-up on the opposite slope is 149 m a.s.l., which is 73 m above the present valley floor. Taking into account the estimate of the deposit thickness (27 m, Table 1), the maximum run-up height is about 100 m. This run-up yields a velocity of 44 m/s, in agreement with the velocity estimate made from runout model (40 s).

The spatial extents of the mapped and modeled rock-avalanche deposits are in good agreement. The maximum extent of the mapped deposit (the isolated hills) indicates a Fahrböschung angle of 17.7°, and the spatial extent of modeled particles yields a value of 17.5°. Similarly, there is good agreement between the two Fahrböschung values in the run-up area—23.3° (mapped deposit) and 24.0° (modeled runout) (Table 5).

Fig. 12 presents results of an alternative runout modeling of the first rock avalanche using the same model parameters but only one type of rheology for the valley-fill sediments (Table 3). This model was used to test the dynamics of a rock avalanche propagating into a dry valley. Although the model can simulate the run-up and the extent of the continuous deposit (A1 and A2) it cannot reproduce the discontinuous deposit of the isolated hills (A3).

Table 5
Runout characteristics for rock-avalanches modeled with DAN3D.

Event	Model volume (10^6 m^3)	Fahrböschung (°)		Travel angle (°)
		Map	Model	
1st rock avalanche (run-up)	15.1	17.7 (23.3)	17.5 (24.0)	27.3
2nd rock avalanche	5.4	24.5	23.7	29.1
3rd rock avalanche	0.3	28.2	28.6	29.6

Notes: Fahrböschung is determined using the most distal modeled particle distribution or mapped debris, respectively. Volume and travel angle are calculated during the simulations.

6.2. Second rock avalanche

Dynamic runout modeling of the second rock avalanche (initial volume 5.4×10^6 m^3) was performed using DAN3D (Fig. 13, Tables 3 and 4). The fragmented rock mass moved over talus and onto the deposit of the first rock avalanche. At 40 s the mass suddenly decelerates upon transitioning from talus to the older rock-avalanche deposit. At 80 s the bulk of mass has come to rest. The model reproduces the mapped spatial extent of the rock-avalanche deposit C. The Fahrböschung angles for the deposit (24.5° for the mapped deposit and 23.7° for the modeled extent) are in agreement (Table 5).

6.3. Third rock avalanche

Finally, the runout of the third rock-avalanche (initial volume of 0.3×10^6 m^3) was modeled with DAN3D (Fig. 14, Tables 3 and 4). The mass propagated over talus and onto the older rock-avalanche deposits. The event lasted about 80 s. The model reproduced the spatial extent of the mapped deposit D. The Fahrböschung angle of the mapped deposit (28.2°) agrees with that of the modeled extent (28.6°) (Table 5).

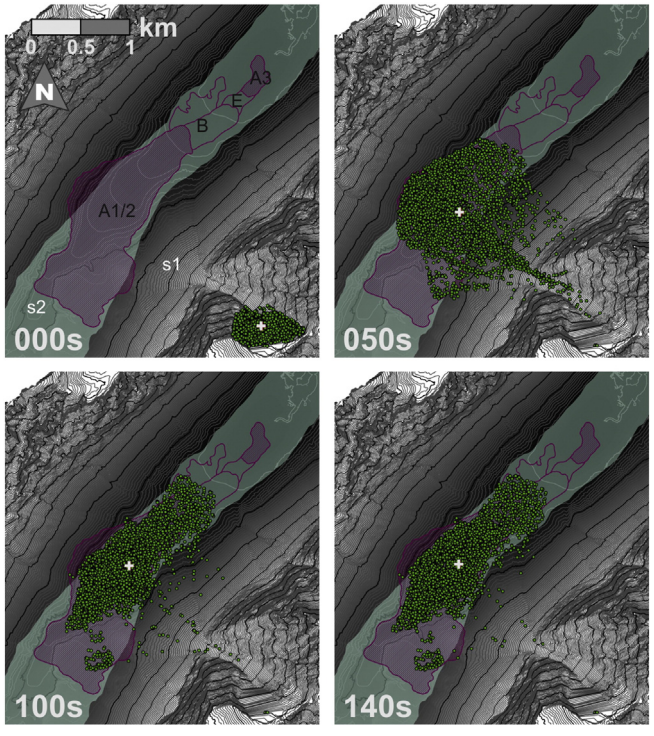

Fig. 12. Simulation of the first rock avalanche with DAN3D assuming a single type of substrate. See caption of Fig. 11 for details.

Please cite this article as: Schleier, M., et al., Subaqueous rock-avalanche deposits exposed by post-glacial isostatic rebound, Innfjorddalen, Western Norway, Geomorphology (2016), http://dx.doi.org/10.1016/j.geomorph.2016.08.024

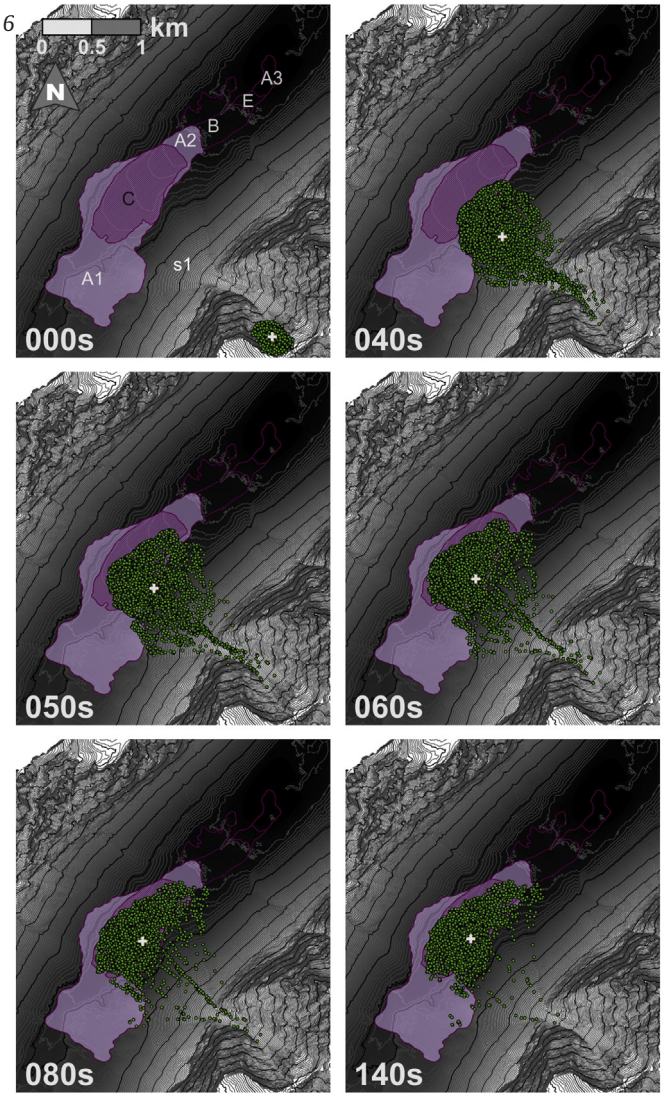

Fig. 13. Simulation of the second rock avalanche with DAN3D. See caption of Fig. 11 for details (no color, s1: bedrock and talus; light polygon, A1, A2: first rock-avalanche deposit; hachured polygon, C: second rock avalanche; outlined polygon, A3, B, E: first rock avalanche and deformed and undeformed valley-fill sediments). (For interpretation of the references to color in this figure legend, the reader is referred to the web version of this article.)

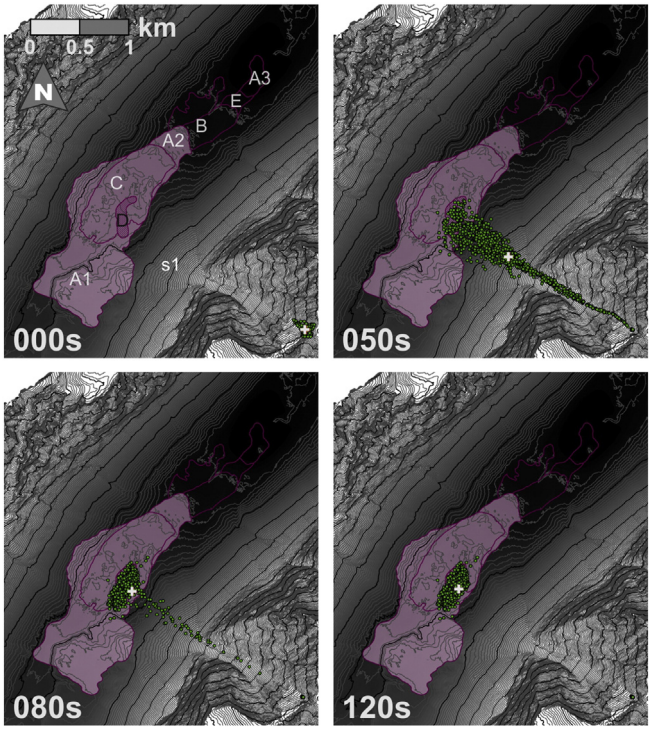

Fig. 14. Simulation of the third rock avalanche with DAN3D. See caption of Fig. 11 for details (no color, s1: talus; light polygon, A1, A2, C: older rock-avalanche deposits; hachured polygon, D: third rock avalanche; outlined polygon, A3, C, B, E: first and second rock avalanche and deformed and undeformed valley-fill sediments). (For interpretation of the references to color in this figure legend, the reader is referred to the web version of this article.)

The main limiting factors for dynamic runout modeling with DAN3D are related to the topographic datasets (e.g., initial volume and runout path) and the applied mechanical properties (Hungr and Evans, 1996; McDougall and Hungr, 2004; Hungr and McDougall, 2009). These uncertainties could be reduced with more thorough interpretation of field data, with further constraints on the topography of source area and deposits, and by calibrating the model calibration through back-analyses. The complexity of the paleoenvironment in which the rock avalanches happened introduces additional uncertainties in modeling, in the case of Innfjorddalen, especially for the first rock avalanche. Nevertheless, there was agreement between the mapped extents, Fahrböschung angles and velocities, and the values for the model parameters (friction coefficient of 0.1 and turbulence coefficient of 500 m/s^2) are consistent with those recommended by Hungr and Evans (1996) and McDougall (2006) for typical rock avalanches (Table 3). Thus, the numerical runout modeling supports the interpretation of landforms and paleoenvironments based on geomorphic evidence and TCN dating.

7. Regional relevance of the findings

This study provides improved knowledge on local valley development in Innfjorddalen. In addition, the findings have broader regional significance. The TCN ages of the first (~14.3 ka.) and second (~8.79 ka) rock avalanche are similar to the ages of two large rock avalanches in Innerdalen Valley about 70 km WNW of Innfjorddalen (~14.1 ka and ~7.97 ka) (Schleier et al., 2015). In contrast, the older two rock avalanches happened in very different environments, specifically onto a glacier at Innderdalen and into a former fjord at Innfjorddalen. At both sites the older two rock avalanches occurred soon after the rock slopes were deglaciated following the decay of the Scandinavian ice sheet (as compared to Hughes et al., 2016). A similar occurrence of rock avalanches during deglaciation has been documented in the Storfjord area just south of the study area (Böhme et al., 2015). Therefore, dating late-glacial rock avalanches could help trace the decay of the Scandinavian ice sheet. Moreover, the similarities in the ages of the rock avalanches at Innfjorddalen and Innerdalen may have implications for triggering mechanisms, such as, climatic impact or seismicity, which need to be compared with other datasets.

Furthermore, the TCN ages of the most distal part of the isolated hills of rock-avalanche debris in Innfjorddalen can be used to improve understanding of post-glacial uplift in Western Norway. In addition, the difference in the TCN age of about 10.4 ka for deposits interpreted to be equivalent in age (deposits A1 and A3) indicates that effects like glacio-isostatic uplift or subsidence could influence the results of surface-exposure dating.

8. Conclusions

We describe and interpret three rock avalanches in Innfjorddalen Valley, Western Norway. The oldest of the three rock avalanches impacted water-saturated sediments in a shallow fjord. The deposits

Please cite this article as: Schleier, M., et al., Subaqueous rock-avalanche deposits exposed by post-glacial isostatic rebound, Innfjorddalen, Western Norway, Geomorphology (2016), http://dx.doi.org/10.1016/j.geomorph.2016.08.024

have become exposed above present sea level due to glacio-isostatic rebound. Surface-exposure dating (^{10}Be) and numerical runout modeling (DAN3D) support the interpretation.

The three rock avalanches emplaced a total of 22.0 × 10^6 m^3 of blocky debris on the floor of Innfjorddalen Valley from the same source on Gråfonnfjellet Mountain: one with a volume of 15.1 × 10^6 m^3 at 14.3 ± 1.4 ka, a second of 5.4 × 10^6 m^3 at 8.79 ± 0.94 ka, and a third of 0.3 × 10^6 m^3 in 1611–12 CE. Additionally, one or more rock avalanches with a total volume of 25.0 × 10^6 m^3 may have occurred during or prior to the last Pleistocene glaciation.

The rock avalanches are recorded as a succession of continuous and discontinuous blocky deposits over an area of 1.44 km^2. The special case in Innfjorddalen is that the first rock avalanche entered a fjord and now is preserved as a blocky deposit lying on and in front of a marine terrace. Thus, it occurred under subaqueous conditions. Associated effects including undrained loading and secondary flow increased the runout of the rock avalanche and left complex deposits including isolated hills of rock-avalanche debris (tomas) that are separated by 700 m from the main continuous rock-avalanche deposit by deformed and apparently undeformed valley-fill sediments.

Innfjorddalen Valley was at least ice-free by 14.3 ka. Post-glacial uplift of the area was in total 120 m after ~14.3 ka and, with higher uncertainty, about 15 m after ~3.9 ka. Post-glacial isostatic uplift is responsible for a discrepancy of about 10.4 ka in the ^{10}Be exposure ages of two parts of a deposit interpreted to be contemporaneous.

Acknowledgements

We thank the Norwegian Water Resources and Energy Directorate (NVE) for financial support for field work and data analyses under the project “Rock avalanche mapping in Møre og Romsdal County”. This paper is based on a sub-chapter of the senior author's doctoral thesis. ^{10}Be sample target chemistry was completed by G. Yang at Dalhousie Geochronology Centre, (Halifax, Canada) with partial support through the NSERC–MRS grant to JCG. AMS analyses were done by S. Zimmerman at CAMS-LLNL (Lawrence Livermore National Lab, Livermore, USA). The 2003 sample was prepared and analyzed at GeoForschungsZentrum (GFZ) Potsdam, Germany and at Labor für Ionenstrahlphysik (LIP) at ETH Zurich, Switzerland. Be targets were prepared by S. Ivy-Ochs, and AMS measurements were made by P. Kubik. We acknowledge Prof. O. Hungr for providing the software code DAN3D. We thank the participants of the field trip during the 3rd Slope Tectonics Conference in 2014 for their useful discussions, and the anonymous reviewers and J.J. Clague for their helpful comments and edits on the manuscript.

References

Abele, G., 1974. Bergstürze in den Alpen, ihre Verbreitung, Morphologie und Folgeerscheinungen. Wiss. Alpenvereinshefte 25 (230 pp.).

Abele, G., 1991. Durch Bergstürze mobilisierte Muren und durch Muren transportierte Bergsturzmassen. Österr. Geogr. Ges., Zweigverein Innsbruck, Jahresber. 1989 (1990), 33–39.

Ballantyne, C.K., Stone, J.O., Fifield, L.K., 1998. Cosmogenic Cl-36 dating of postglacial landsliding at The Storr, Isle of Skye, Scotland. The Holocene 8, 347–351. http://dx.doi.org/10.1191/095968398666797200.

Blais-Stevens, A., Hermanns, R.L., Jermyn, C., 2011. A 36Cl age determination for Mystery Creek rock avalanche and its implications in the context of hazard assessment, British Columbia, Canada. Landslides 8, 407–416. http://dx.doi.org/10.1007/s10346-011-0261-0.

Blikra, L.H., Braathen, A., Anda, E., Stalsberg, K., Longva, O., 2002. Rock avalanches, gravitational bedrock fractures and neotectonic faults onshore northern West Norway: Examples, regional distribution and triggering mechanisms. Geological Survey of Norway Report 2002.016 (48 pp.).

Blikra, L.H., Longva, O., Braathen, A., Anda, E., Dehls, J.F., Stalsberg, K., 2006. Rock slope failures in Norwegian fjord areas: examples, spatial distribution and temporal pattern. In: Evans, S.G., Scarascia Mugnozza, G., Strom, A., Hermanns, R.L. (Eds.), Landslides from Massive Rock Slope FailureNATO Science Series IV: Earth and Environmental Sciences vol. 49. Springer, Dordrecht, pp. 475–496.

Böhme, M., Saintot, A., Henderson, I.H.C., Henriksen, H., Hermanns, R.L., 2011. Rock slope instabilities in Sogn and Fjordane County, Norway: a detailed structural and geomorphological analysis. In: Jaboyedoff, M. (Ed.), Slope Tectonics. Geological Society, London, Special Publications vol. 351, pp. 97–111. http://dx.doi.org/10.1144/sp351.5.

Böhme, M., Oppikofer, T., Longva, O., Jaboyedoff, M., Hermanns, R.L., Derron, M.H., 2015. Analyses of past and present rock slope instabilities in a fjord valley: implications for hazard estimations. Geomorphology 248, 464–474. http://dx.doi.org/10.1016/j.geomorph.2015.06.045.

Borchers, B., Marrero, S., Balco, G., Caffee, M., Goehring, B., Lifton, N., Nishiizumi, K., Phillips, F., Schaefer, J., Stone, J., 2016. Geological calibration of spallation production rates in the CRONUS-Earth project. Quat. Geochronol. 31, 188–198. http://dx.doi.org/10.1016/j.quageo.2015.01.009.

Boultbee, N., Stead, D., Schwab, J., Geertsema, M., 2006. The Zymoetz River rock avalanche, June 2002, British Columbia, Canada. Eng. Geol. 83, 76–93. http://dx.doi.org/10.1016/j.enggeo.2005.06.038.

Braathen, A., Blikra, L.H., Berg, S.S., Karlsen, F., 2004. Rock-slope failures in Norway; type, geometry, deformation mechanisms and stability. Nor. J. Geol. 84, 67–88.

Crandell, D.R., Fahnestock, R.K., 1965. Rockfalls and avalanches from Little Tahoma Peak on Mount Rainier, Washington. U.S. Geol. Surv. Bull. 1221-A 30 pp.

Crosta, G.B., Chen, H., Lee, C.F., 2004. Replay of the 1987 Val Pola Landslide, Italian Alps. Geomorphology 60, 127–146. http://dx.doi.org/10.1016/j.geomorph.2003.07.015.

Crosta, G.B., Imposimato, S., Roddeman, D., 2009a. Numerical modelling of entrainment/deposition in rock and debris-avalanches. Eng. Geol. 109, 135–145. http://dx.doi.org/10.1016/j.enggeo.2008.10.004.

Crosta, G.B., Imposimato, S., Roddeman, D., 2009b. Numerical modeling of 2-D granular step collapse on erodible and nonerodible surface. J. Geophys. Res. Earth Surf. 114. http://dx.doi.org/10.1029/2008jf001186 (19 pp.).

De Blasio, F.V., 2014. Friction and dynamics of rock avalanches travelling on glaciers. Geomorphology 213, 88–98. http://dx.doi.org/10.1016/j.geomorph.2014.01.001.

Dehls, J.F., Olesen, O., Bungum, H., Hicks, E.C., Lindholm, C.D., Riis, F., 2000. Neotectonic Map: Norway and Adjacent Areas. Geological Survey of Norway, Trondheim.

Delaney, K., Evans, S., 2014. The 1997 Mount Munday landslide (British Columbia) and the behaviour of rock avalanches on glacier surfaces. Landslides 11, 1019–1036. http://dx.doi.org/10.1007/s10346-013-0456-7.

Dufresne, A., 2012. Granular flow experiments on the interaction with stationary runout path materials and comparison to rock avalanche events. Earth Surf. Process. Landf. 37, 1527–1541. http://dx.doi.org/10.1002/esp.3296.

Dufresne, A., Davies, T.R., 2009. Longitudinal ridges in mass movement deposits. Geomorphology 105, 171–181. http://dx.doi.org/10.1016/j.geomorph.2008.09.009.

Dufresne, A., Salinas, S., Siebe, C., 2010a. Substrate deformation associated with the Jocotitlán edifice collapse and debris avalanche deposit, Central México. J. Volcanol. Geotherm. Res. 197, 133–148. http://dx.doi.org/10.1016/j.jvolgeores.2010.02.019.

Dufresne, A., Davies, T.R., McSaveney, M.J., 2010b. Influence of runout-path material on emplacement of the Round Top rock avalanche, New Zealand. Earth Surf. Process. Landf. 35, 190–201. http://dx.doi.org/10.1002/esp.1900.

Dunning, S., Armitage, P.J., 2011. The grain-size distribution of rock-avalanche deposits: implications for natural dam stability. In: Evans, S.G., Hermanns, R.L., Strom, A., Scarascia-Mugnozza, G. (Eds.), Natural and Artificial Rockslide DamsLecture Notes in Earth Sciences vol. 133. Springer, Berlin/Heidelberg, pp. 479–498.

Dunning, S.A., Mitchell, W.A., Rosser, N.J., Petley, D.N., 2007. The Hattian Bala rock avalanche and associated landslides triggered by the Kashmir earthquake of 8 October 2005. Eng. Geol. 93, 130–144. http://dx.doi.org/10.1016/j.enggeo.2007.07.003.

Erismann, T.H., Abele, G., 2001. Dynamics of Rockslides and Rockfalls. Springer, Berlin (316 pp.).

Evans, S.G., Clague, J.J., Woodsworth, G.J., Hungr, O., 1989. The Pandemonium Creek rock avalanche, British Columbia. Can. Geotech. J. 26, 427–446. http://dx.doi.org/10.1139/t89-056.

Evans, S.G., Scarascia Mugnozza, G., Strom, A.L., Hermanns, R.L., Ischuk, A., Vinnichenko, S., 2006. Landslides from massive rock slope failure and associated phenomena. In: Evans, S.G., Scarascia Mugnozza, G., Strom, A., Hermanns, R.L. (Eds.), Landslides from Massive Rock Slope FailureNATO Science Series IV: Earth and Environmental Sciences vol. 49. Springer, Dordrecht, pp. 3–52.

Evans, S.G., Bishop, N.F., Fidel Smoll, L., Valderrama Murillo, P., Delaney, K.B., Oliver-Smith, A., 2009. A re-examination of the mechanism and human impact of catastrophic mass flows originating on Nevado Huascarán, Cordillera Blanca, Peru in 1962 and 1970. Eng. Geol. 108, 96–118. http://dx.doi.org/10.1016/j.enggeo.2009.06.020.

Evans, S.G., Delaney, K.B., Hermanns, R.L., Strom, A., Scarascia-Mugnozza, G., 2011. The formation and behaviour of natural and artificial rockslide dams; implications for engineering performance and hazard management. In: Evans, S.G., Hermanns, R.L., Strom, A., Scarascia-Mugnozza, G. (Eds.), Natural and Artificial Rockslide DamsLecture Notes in Earth Sciences vol. 133. Springer, Berlin/Heidelberg, pp. 1–75.

Fjeldskaar, W., Lindholm, C., Dehls, J.F., Fjeldskaar, I., 2000. Postglacial uplift, neotectonics and seismicity in Fennoscandia. Quat. Sci. Rev. 19, 1413–1422. http://dx.doi.org/10.1016/S0277-3791(00)00070-6.

Fredin, O., Bergstrøm, B., Eilertsen, R., Hansen, L., Longva, O., Nesje, A., Sveian, H., 2013. Glacial landforms and Quaternary landscape development in Norway. In: Olsen, L., Fredin, O., Olesen, O. (Eds.), Quaternary Geology of Norway. Geological Survey of Norway Special Publication 13, pp. 5–25 Trondheim.

Furseth, A., 2006. Skredulykker i Norge. Tun Forlag, Oslo.

Gosse, J.C., Phillips, F.M., 2001. Terrestrial in situ cosmogenic nuclides: theory and application. Quat. Sci. Rev. 20, 1475–1560. http://dx.doi.org/10.1016/s0277-3791(00)00171-2.

Hacker, B.R., Andersen, T.B., Johnston, S., Kylander-Clark, A.R.C., Peterman, E.M., Walsh, E.O., Young, D., 2010. High-temperature deformation during continental-margin subduction and exhumation: the ultrahigh-pressure Western Gneiss Region of Norway. Tectonophysics 480, 149–171. http://dx.doi.org/10.1016/j.tecto.2009.08.012.

Please cite this article as: Schleier, M., et al., Subaqueous rock-avalanche deposits exposed by post-glacial isostatic rebound, Innfjorddalen, Western Norway, Geomorphology (2016), http://dx.doi.org/10.1016/j.geomorph.2016.08.024

Hansen, L., Sveian, H., Olsen, L., Høgaas, F., Rindstad, B.I., Wiig, T., Lyche, E., 2012. The marine limit as a basis for mapping of landslide susceptibility in fine-grained, fjord deposits, onshore Norway. In: Eberhardt, E., Froese, C., Turner, K., Leroueil, S. (Eds.), Landslides and Engineered Slopes: Protecting Society Through Improved Understanding. Taylor & Francis Group, London, pp. 1833–1838.

Hansen, L., Høgaas, F., Sveian, H., Olsen, L., Rindstad, B.I., 2014. Quaternary geology as a basis for landslide susceptibility assessment in fine-grained, marine deposits, onshore Norway. In: L'Heureux, J.-S. (Ed.), Landslides in Sensitive Clays: From Geosciences to Risk ManagementAdvances in Natural and Technological Hazards Research vol. 36. Springer Science & Business Media, Dordrecht, pp. 369–381.

Heim, A., 1932. Bergsturz und Menschenleben. Beibl. Vierteljahr. Naturforsch.Ges. Zürich 77 (218 pp.).

Henderson, I.H.C., Saintot, A., 2011. Regional spatial variations in rockslide distribution from structural geology ranking: an example from Storfjorden, western Norway. In: Jaboyedoff, M. (Ed.), Slope Tectonics. Geological Society, London, Special Publications vol. 351, pp. 79–95. http://dx.doi.org/10.1144/sp351.4.

Hermanns, R.L., Longva, O., 2012. Rapid rock-slope failures. In: Clague, J.J., Stead, D. (Eds.), Landslides: Types, Mechanisms and Modeling. Cambridge University Press, Cambridge, pp. 59–70.

Hermanns, R.L., Trauth, M.H., Niedermann, S., McWilliams, M., Strecker, M.R., 2000. Tephrochronologic constraints on temporal distribution of large landslides in NW-Argentina. J. Geol. 108, 35–52.

Hermanns, R.L., Niedermann, S., Garcia, A.V., Gomez, J.S., Strecker, M.R., 2001. Neotectonics and catastrophic failure of mountain fronts in the southern intra-Andean Puna Plateau, Argentina. Geology 29, 619–622. http://dx.doi.org/10.1130/0091-7613(2001)029<0619:nacfom>2.0.co;2.

Hermanns, R.L., Niedermann, S., Ivy-Ochs, S., Kubik, P.W., 2004. Rock avalanching into a landslide-dammed lake causing multiple dam failure in Las Conchas valley (NW Argentina) - evidence from surface exposure dating and stratigraphic analyses. Landslides 1, 113–122. http://dx.doi.org/10.1007/s10346-004-0013-5.

Hermanns, R.L., Blikra, L.H., Naumann, M., Nilsen, B., Panthi, K.K., Stromeyer, D., Longva, O., 2006. Examples of multiple rock-slope collapses from Köfels (Ötz valley, Austria) and western Norway. Eng. Geol. 83, 94–108. http://dx.doi.org/10.1016/j.enggeo.2005.06.026.

Hermanns, R.L., Hewitt, K., Strom, A., Evans, S.G., Dunning, S.A., Scarascia-Mugnozza, G., 2011. The classification of rockslide dams. In: Evans, S.G., Hermanns, R.L., Strom, A., Scarascia-Mugnozza, G. (Eds.), Natural and Artificial Rockslide DamsLecture Notes in Earth Sciences Vol. 133. Springer, Berlin/Heidelberg, pp. 581–593.

Hermanns, R.L., Hansen, L., Sletten, K., Böhme, M., Bunkholt, H.S.S., Dehls, J.F., Eilertsen, R.S., Fischer, L., L'Heureux, J.-S., Høgaas, F., Nordahl, B., Oppikofer, T., Rubensdotter, L., Solberg, I.-L., Stalsberg, K., Yugsi Molina, F.X., 2012a. Systematic geological mapping for landslide understanding in the Norwegian context. In: Eberhardt, E., Froese, C., Turner, K., Leroueil, S. (Eds.), Landslides and Engineered Slopes: Protecting Society through Improved Understanding. Taylor & Francis Group, London, pp. 265–271.

Hermanns, R.L., Redfield, T.F., Bunkholt, H.S.S., Fischer, L., Oppikofer, T., Gosse, J., Eiken, T., 2012b. Cosmogenic nuclide dating of slow moving rockslides in Norway in order to assess long-term slide velocities. In: Eberhardt, E., Froese, C., Turner, K., Leroueil, S. (Eds.), Landslides and Engineered Slopes: Protecting Society Through Improved Understanding. Taylor & Francis Group, London, pp. 849–854.

Hermanns, R.L., Fauqué, L., Wilson, C.G.J., 2014. ^{36}Cl terrestrial cosmogenic nuclide dating suggests late Pleistocene to Early Holocene mass movements on the south face of Aconcagua mountain and in the Las Cuevas–Horcones valleys, Central Andes, Argentina. Geol. Soc. Lond., Spec. Publ. 399. http://dx.doi.org/10.1144/sp399.19.

Hewitt, K., 1998. Catastrophic landslides and their effects on the Upper Indus streams, Karakoram Himalaya, northern Pakistan. Geomorphology 26, 47–80. http://dx.doi.org/10.1016/S0169-555X(98)00051-8.

Hewitt, K., 2009a. Rock avalanches that travel onto glaciers and related developments, Karakoram Himalaya, Inner Asia. Geomorphology 103 (1), 66–79. http://dx.doi.org/10.1016/j.geomorph.2007.10.017.

Hewitt, K., 2009b. Catastrophic rock slope failures and late Quaternary developments in the Nanga Parbat-Haramosh Massif, Upper Indus basin, northern Pakistan. Quat. Sci. Rev. 28, 1055–1069. http://dx.doi.org/10.1016/j.quascirev.2008.12.019.

Hewitt, K., Clague, J.J., Orwin, J.F., 2008. Legacies of catastrophic rock slope failures in mountain landscapes. Earth Sci. Rev. 87, 1–38. http://dx.doi.org/10.1016/j.earscirev.2007.10.002.

Hewitt, K., Gosse, J., Clague, J.J., 2011. Rock avalanches and the pace of late Quaternary development of river valleys in the Karakoram Himalaya. Geol. Soc. Am. Bull. 123, 1836–1850. http://dx.doi.org/10.1130/B30341.1.

Hughes, A.L.C., Gyllencreutz, R., Lohne, Ø.S., Mangerud, J., Svendsen, J.I., 2016. The last Eurasian ice sheets – a chronological database and time-slice reconstruction, DATED-1. Boreas 45, 1–45. http://dx.doi.org/10.1111/bor.12142.

Hungr, O., 2006. Rock avalanche occurrence, process and modelling. In: Evans, S.G., Scarascia Mugnozza, G., Strom, A., Hermanns, R.L. (Eds.), Landslides from Massive Rock Slope FailureNATO Science Series IV: Earth and Environmental Sciences vol. 49. Springer, Dordrecht, pp. 243–266.

Hungr, O., Evans, S.G., 1996. Rock avalanche runout prediction using a dynamic model. In: Senneset, K. (Ed.), Proceedings of the 7th International Symposium on Landslides. A.A. Balkema, Rotterdam, pp. 233–238.

Hungr, O., Evans, S.G., 2004. Entrainment of debris in rock avalanches: an analysis of a long run-out mechanism. Geol. Soc. Am. Bull. 116, 1240–1252. http://dx.doi.org/10.1130/b25362.1.

Hungr, O., McDougall, S., 2009. Two numerical models for landslide dynamic analysis. Comput. Geosci. 35, 978–992. http://dx.doi.org/10.1016/j.cageo.2007.12.003.

Ivy-Ochs, S., Poschinger, A.v., Synal, H.A., Maisch, M., 2009. Surface exposure dating of the Flims landslide, Graubünden, Switzerland. Geomorphology 103, 104–112. http://dx.doi.org/10.1016/j.geomorph.2007.10.024.

Legros, F., 2002. The mobility of long-runout landslides. Eng. Geol. 63, 301–331. http://dx.doi.org/10.1016/s0013-7952(01)00090-4.

Lifton, N., Sato, T., Dunai, T.J., 2014. Scaling in situ cosmogenic nuclide production rates using analytical approximations to atmospheric cosmic-ray fluxes. Earth Planet. Sci. Lett. 386, 149–160. http://dx.doi.org/10.1016/j.epsl.2013.10.052.

Longva, O., Blikra, L.H., Dehls, J.F., 2009. Rock avalanches - distribution and frequencies in the inner part of Storfjorden, Møre og Romsdal County, Norway. Geological Survey of Norway Report 2009.002 (23 pp.).

Luna, B.Q., Remaître, A., van Asch, T.W.J., Malet, J.P., van Westen, C.J., 2012. Analysis of debris flow behavior with a one dimensional run-out model incorporating entrainment. Eng. Geol. 128, 63–75. http://dx.doi.org/10.1016/j.enggeo.2011.04.007.

Maiforth, J., 2010. Kulturminner på Flakk (in Norwegian) (Master thesis) Norges teknisk-naturvitenskapelige universitet, Trondheim, Norway.

Masera, D., Giardino, M., Perotti, L., Poschinger, A.v., Calhoun, N., Clague, J.J., 2014. Application of geomorphology and geomatics in the study of the Flims and Tamins landslides, Switzerland. In: Hermanns, R.L., Liinamaa-Dehls, A., Dehls, J.F., Oppikofer, T. (Eds.), 3rd Slope Tectonics Conference: Program and Abstract Book. Geological Survey of Norway Report 2014.030, p. 42.

Mauring, E., Lauritsen, T., Tønnesen, J.F., 1998. Georadarmålinger I formindelse med undersøkelser av fjellskred I Tafjord, Romsdalen, Hellesylt og Innfjorden, Møre og Romsdal. Geological Survey of Norway Report 98.047.

McDougall, S., 2006. A New Continuum Dynamic Model for the Analysis of Extremely Rapid Landslide Motion Across Complex 3D Terrain Doctoral thesis The University of British Columbia, Vancouver, Canada (253 pp.).

McDougall, S., Hungr, O., 2004. A model for the analysis of rapid landslide motion across three-dimensional terrain. Can. Geotech. J. 41, 1084–1097. http://dx.doi.org/10.1139/t04-052.

McDougall, S., Hungr, O., 2005. Dynamic modelling of entrainment in rapid landslides. Can. Geotech. J. 42, 1437–1448. http://dx.doi.org/10.1139/t05-064.

NGU, 2009. Kartblad NR 1319 IV: Georadaropptak G1 og G2, Innfjorddalen. Norges geologiske undersøkelse (unpublished dataset).

NGU, 2015. Online database: Nasjonal løsmassedatabase - Standardkart: marin grense. Norges geologiske undersøkelse http://geo.ngu.no/kart/losmasse/ accessed 13 Jan 2015.

Olesen, O., Bungum, H., Dehls, J., Lindholm, C., Pascal, C., Roberts, D., 2013. Neotectonics, seismicity and contemporary stress field in Norway – mechanisms and implications. In: Olsen, L., Fredin, O., Olesen, O. (Eds.), Quaternary Geology of Norway. Geological Survey of Norway Special Publication 13, pp. 145–174 (Trondheim).

Olsen, L., Sveian, H., Bergstrøm, B., Ottesen, D., Rise, L., 2013. Quaternary glaciations and their variations in Norway and on the Norwegian continental shelf. In: Olsen, L., Fredin, O., Olesen, O. (Eds.), Quaternary Geology of Norway. Geological Survey of Norway Special Publication 13, pp. 27–78 Trondheim.

Oppikofer, T., Saintot, A., Otterå, S., Hermanns, R.L., Anda, E., Dahle, H., Eiken, T., 2013. Investigations on unstable rock slopes in Møre og Romsdal - status and plans after field surveys in 2012. Geological Survey of Norway Report 2013.014 (324 pp.).

Oppikofer, T., Nordahl, B., Bunkholt, H., Nicolaisen, M., Jarna, A., Iversen, S., Hermanns, R.L., Böhme, M., Yugsi Molina, F.X., 2015. Database and online map service on unstable rock slopes in Norway — from data perpetuation to public information. Geomorphology 249, 69–81. http://dx.doi.org/10.1016/j.geomorph.2015.08.005.

Pedrazzini, A., Froese, C.R., Jaboyedoff, M., Hungr, O., Humair, F., 2012. Combining digital elevation model analysis and run-out modeling to characterize hazard posed by a potentially unstable rock slope at Turtle Mountain, Alberta, Canada. Eng. Geol. 128, 76–94. http://dx.doi.org/10.1016/j.enggeo.2011.03.015.

Pettijohn, E.J., Doornkamp, J.C., 1973. Sand and Sandstone. Springer-Verlag, Berlin (618 pp.).

Pirulli, M., 2009. The Thurwieser rock avalanche (Italian Alps): description and dynamic analysis. Eng. Geol. 109, 80–92. http://dx.doi.org/10.1016/j.enggeo.2008.10.007.

Poschinger, A.v., 2002. Large rockslides in the Alps: a commentary on the contribution of G. Abele (1937–1994) and a review of some recent developments. In: Evans, S.G., DeGraff, J.V. (Eds.), Catastrophic Landslides: Effects, Occurrence, and Mechanisms. Geological Society of America Reviews in Engineering Geology, Boulder, Colorado, pp. 237–255.

Poschinger, A.v., Kippel, T., 2009. Alluvial deposits liquefied by the Flims rock slide. Geomorphology 103, 50–56. http://dx.doi.org/10.1016/j.geomorph.2007.09.016.

Poschinger, A.v., Wassmer, P., Maisch, M., 2006. The Flims rockslide: history of interpretation and new insights. In: Evans, S.G., Scarascia Mugnozza, G., Strom, A., Hermanns, R.L. (Eds.), Landslides from Massive Rock Slope FailureNATO Science Series IV: Earth and Environmental Sciences vol. 49. Springer, Dordrecht, pp. 329–356.

Saintot, A., Henderson, I.H.C., Derron, M.-H., 2011. Inheritance of ductile and brittle structures in the development of large rock slope instabilities: examples from western Norway. In: Jaboyedoff, M. (Ed.), Slope Tectonics. Geological Society, London, Special Publications vol. 351, pp. 27–78. http://dx.doi.org/10.1144/sp351.3.

Saintot, A., Oppikofer, T., Derron, M.H., Henderson, I., 2012. Large gravitational rock slope deformation in Romsdalen Valley (Western Norway). Rev. Asoc. Geol. Argent. 69, 354–371.

Scheidegger, A.E., 1973. On the prediction of the reach and velocity of catastrophic landslides. Rock Mech. 5, 231–236.

Schleier, M., Hermanns, R.L., Rohn, J., 2013. Spatial distribution of rockslide deposits and their morphological features suggest timing and palaeo-environmental conditions for rock slope failures in Innerdalen and Innfjorddalen, Møre og Romsdal county, western Norway. In: Genevois, R., Prestininzi, A. (Eds.), International Conference on Vajont 1963–2013: Thoughts and Analyses After 50 Years Since the Catastrophic

Please cite this article as: Schleier, M., et al., Subaqueous rock-avalanche deposits exposed by post-glacial isostatic rebound, Innfjorddalen, Western Norway, Geomorphology (2016), http://dx.doi.org/10.1016/j.geomorph.2016.08.024

Landslide. Italian Journal of Engineering Geology and Environment, Book Series 6, pp. 493–505.
Schleier, M., Hermanns, R.L., Rohn, J., Gosse, J., 2015. Diagnostic characteristics and paleodynamics of supraglacial rock avalanches, Innerdalen, Western Norway. Geomorphology 245, 23–39. http://dx.doi.org/10.1016/j.geomorph.2015.04.033.
Schleier, M., Hermanns, R.L., Krieger, I., Oppikofer, T., Eiken, T., Rønning, J.S., Rohn, J., 2016. Gravitational reactivation of a pre-existing post-Caledonian fault system: the deep-seated gravitational slope deformation at Middagstinden, western Norway. Nor. J. Geol. 96, 23.
Seljesæter, S., 2010. Diskusjon av opprinnelsen til deformasjonsstrukturane i dalbotnsedimenta i Innfjorden (in Norwegian). unpublished Master thesis, Norges teknisk-naturvitenskapelige universitet, Trondheim, Norway, (113 pp).
Shugar, D.H., Rabus, B.T., Clague, J.J., Capps, D.M., 2012. The response of Black Rapids Glacier, Alaska, to the Denali earthquake rock avalanches. J. Geophys. Res. Earth Surf. 117, F01006. http://dx.doi.org/10.1029/2011jf002011.
Shulmeister, J., Davies, T.R., Evans, D.J.A., Hyatt, O.M., Tovar, D.S., 2009. Catastrophic landslides, glacier behaviour and moraine formation – a view from an active plate margin. Quat. Sci. Rev. 28, 1085–1096. http://dx.doi.org/10.1016/j.quascirev.2008.11.015.
Soldati, M., Corsini, A., Pasuto, A., 2004. Landslides and climate change in the Italian Dolomites since the Late glacial. Catena 55, 141–161. http://dx.doi.org/10.1016/s0341-8162(03)00113-9.
Sollid, J.L., Sørbel, L., 1979. Deglaciation of western Central Norway. Boreas 8, 233–239. http://dx.doi.org/10.1111/j.1502-3885.1979.tb00805.x.
Sosio, R., Crosta, G.B., Hungr, O., 2008. Complete dynamic modeling calibration for the Thurwieser rock avalanche (Italian Central Alps). Eng. Geol. 100, 11–26.
Sosio, R., Crosta, G.B., Chen, J.H., Hungr, O., 2012. Modelling rock avalanche propagation onto glaciers. Quat. Sci. Rev. 47, 23–40. http://dx.doi.org/10.1016/j.quascirev.2012.05.010.
Strom, A., 2006. Morphology and internal structure of rockslides and rock avalanches: grounds and constraints for their modelling. In: Evans, S.G., Scarascia Mugnozza, G., Strom, A., Hermanns, R.L. (Eds.), Landslides from Massive Rock Slope FailureNATO Science Series IV: Earth and Environmental Sciences vol. 49. Springer, Dordrecht, pp. 305–326.
Trauth, M.H., Alonso, R.A., Haselton, K.R., Hermanns, R.L., Strecker, M.R., 2000. Climate change and mass movements in the NW Argentine Andes. Earth Planet. Sci. Lett. 179, 243–256. http://dx.doi.org/10.1016/s0012-821x(00)00127-8.
Tveten, E., Lutro, O., Thorsnes, T., 1998. Geologisk Kart over Norge, Berggrunnskart Ålesund, 1:250,000. Geological Survey of Norway, Trondheim.
Welkner, D., Eberhardt, E., Hermanns, R.L., 2010. Hazard investigation of the Portillo Rock Avalanche site, central Andes, Chile, using an integrated field mapping and numerical modelling approach. Eng. Geol. 114, 278–297. http://dx.doi.org/10.1016/j.enggeo.2010.05.007.

Please cite this article as: Schleier, M., et al., Subaqueous rock-avalanche deposits exposed by post-glacial isostatic rebound, Innfjorddalen, Western Norway, Geomorphology (2016), http://dx.doi.org/10.1016/j.geomorph.2016.08.024